Provided for non-commercial research and education use.
Not for reproduction, distribution or commercial use.

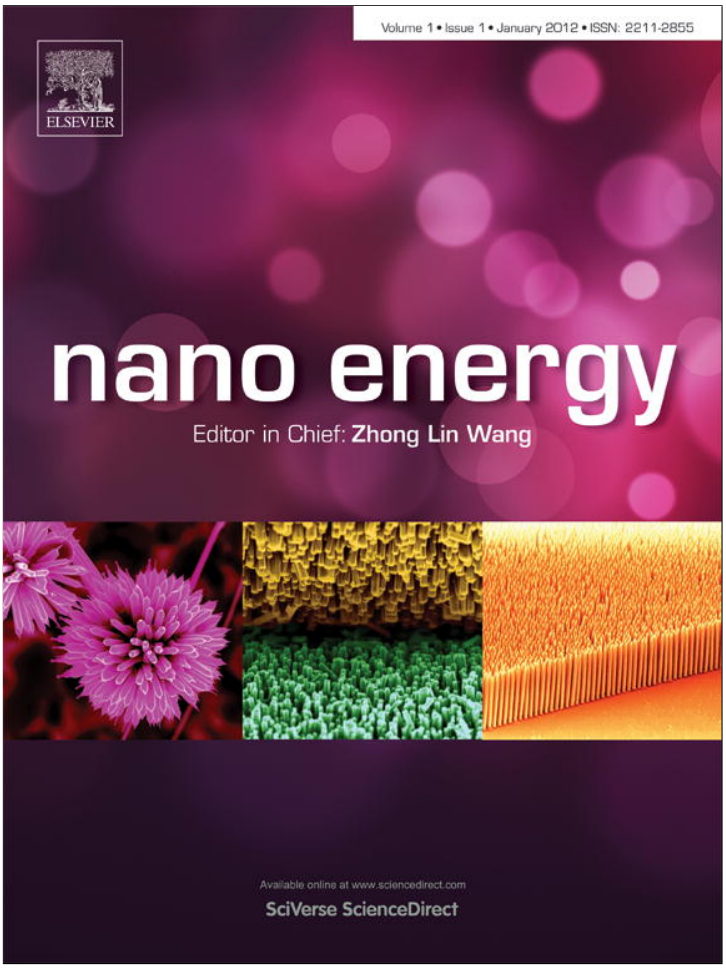

This article appeared in a journal published by Elsevier. The attached copy is furnished to the author for internal non-commercial research and education use, including for instruction at the authors institution and sharing with colleagues.

Other uses, including reproduction and distribution, or selling or licensing copies, or posting to personal, institutional or third party websites are prohibited.

In most cases authors are permitted to post their version of the article (e.g. in Word or Tex form) to their personal website or institutional repository. Authors requiring further information regarding Elsevier's archiving and manuscript policies are encouraged to visit:

http://www.elsevier.com/copyright

Author's personal copy

Nano Energy (2012) 1, 107–131

Available online at www.sciencedirect.com

SciVerse ScienceDirect

journal homepage: www.elsevier.com/locate/nanoenergy

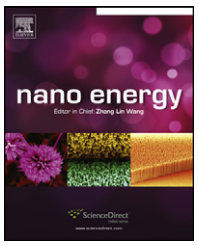

REVIEW

Graphene/metal oxide composite electrode materials for energy storage

Zhong-Shuai Wu[a,b,1], Guangmin Zhou[a,1], Li-Chang Yin[a], Wencai Ren[a], Feng Li[a], Hui-Ming Cheng[a,*]

[a]*Shenyang National Laboratory for Materials Science, Institute of Metal Research, Chinese Academy of Sciences, 72 Wenhua Road, Shenyang 110016, PR China*
[b]*Max Planck Institute for Polymer Research, Ackermannweg 10, 55128 Mainz, Germany*

Received 10 October 2011; received in revised form 8 November 2011; accepted 11 November 2011
Available online 2 December 2011

KEYWORDS
Graphene;
Metal oxide;
Composite;
Energy storage;
Lithium ion battery;
Supercapacitor

Abstract
Recent progress on graphene/metal oxide composites as advanced electrode materials in lithium ion batteries (LIBs) and electrochemical capacitors (ECs) is described, highlighting the importance of synergistic effects between graphene and metal oxides and the beneficial role of graphene in composites for LIBs and ECs. It is demonstrated that, when the composites are used as electrode materials for LIBs and ECs, compared to their individual constituents, graphene/metal oxide composites with unique structural variables such as anchored, wrapped, encapsulated, sandwich, layered and mixed models have a significant improvement in their electrochemical properties such as high capacity, high rate capability and excellent cycling stability. First, an introduction on the properties, synthesis strategies and use of graphene is briefly given, followed by a state-of-the-art review on the preparation of graphene/metal oxide composites and their electrochemical properties in LIBs and ECs. Finally, the prospects and future challenges of graphene/metal oxide composites for energy storage are discussed.
© 2011 Elsevier Ltd. All rights reserved.

Introduction

Graphene is a one-atom-thick sheet of sp^2-bonded carbon atoms in a honeycomb crystal lattice, which is at the cutting-edge of materials science and condensed matter physics research [1–4]. It is the thinnest known material in the world and conceptually a basic build block for constructing many other carbon materials. It can be rolled into one-dimensional carbon nanotubes (CNTs), and stacked into three-dimensional (3D) graphite. With the addition of pentagons it can be wrapped into a spherical fullerene. In one sense, it is the mother of all graphitic materials [3].

In 2004, Geim and Novoselov reported their experimental investigation of the exfoliation, characterization and electronic

*Corresponding author. Tel.: +86 24 23971611; fax: +86 24 2390 3126.
E-mail address: cheng@imr.ac.cn (H.-M. Cheng).
[1]These authors have equally contributed.

2211-2855/$ - see front matter © 2011 Elsevier Ltd. All rights reserved.
doi:10.1016/j.nanoen.2011.11.001

Author's personal copy

properties of this two-dimensional (2D) carbon by repeatedly cleaving graphite with an adhesive tape [1]. Theoretical work on this structure has being carried out for decades [5], but isolated graphene and other 2D atomic layers are considered to be thermodynamically unstable. By using the same top-down approach and starting with other bulk 3D crystals with a layered structure, several stable 2D crystal nanosheets, such as boron nitride, dichalcogenide and Bi-Sr-Ca-Cu-O superconductor, were also produced by an exfoliation process. This finding shows that free-standing 2D crystals do exist and are stable at ambient temperature [6]. Graphene has been already drawn a wealth of research activities in its production, versatile unique properties and many high-tech applications.

Properties of graphene

From the viewpoint of its electronic properties, graphene is a zero-gap semiconductor with unique electronic properties originating from the fact that charge carriers in graphene are described by a Dirac-like equation, rather than the usual Schrödinger equation [2]. As a consequence of its perfect crystal structure, low-energy quasiparticles in it obey a linear dispersion relation, similar to massless relativistic particles. This essential characteristic of a gapless semiconductor has led to many observations of peculiar electronic properties [3,7-9] including ballistic transport, pseudospin chirality based on the "Berry phase", a room-temperature half-integer "chiral" quantum Hall effect, and conductivity without charge carriers, that make it a promising choice for future electronic materials, both as a device and as an interconnect. For example, graphene has the fastest electron mobility of $\sim$15,000 $cm^2 V^{-1} cm^{-1}$ or $10^6\ \Omega$ cm (lower than Ag), a superhigh mobility of temperature-independent charge carriers of 200,000 $cm^2 V^{-1} s^{-1}$ (200 times higher than Si), and an effective Fermi velocity of 10^6 m s^{-1} at room temperature, similar to the speed of light.

More importantly, graphene possesses not only unique electronic properties, but also excellent mechanical, optical, thermal and electrochemical properties that are superior to other carbon allotropes such as graphite, diamond, fullerene and CNTs, as shown in Table 1 [3,4,10-13]. Single-layer graphene has excellent mechanical properties with a Young's modulus of 1.0 TPa and a stiffness of 130 GPa, optical transmittance of $\sim$97.7% (absorbing 2.3% of white light), and superior thermal conductivity of 5000 W $m^{-1} K^{-1}$ (about 100 times that of Cu). It also has a high theoretical specific surface area of 2620 $m^2 g^{-1}$, extreme electrical conductivity and good flexibility. Due to its unique properties, it is speculated that in many applications graphene will out-perform CNTs, graphite, metals and semiconductors where it is used as an individual material or as a component in a hybrid or composite material.

Synthesis of graphene

Since 2004, much work has been related to the synthesis of graphene, because its availability is an important precondition for its use in research and development into possible applications. So far, there are various intriguing strategies for producing single-layer and few-layer graphene that can be broadly categorized into the following six groups:

(i) Micromechanical cleavage of highly oriented pyrolytic graphite or natural graphite flakes using a Scotch tape. It is the first method to be used to produce graphene and is suitable for fundamental research due to the high structural and electronic quality of the graphene produced. This technique allows reliable and easy preparation but suffers from a low yield [1].

Table 1 The properties of graphene and other carbon allotropes.

Carbon allotropes	Graphite	Diamond	Fullerene (C_{60})	Carbon nanotube	Graphene
Hybridized form	sp^2	sp^3	Mainly sp^2	Mainly sp^2	sp^2
Crystal system	Hexagonal	Octahedral	Tetragonal	Icosahedral	Hexagonal
Dimension	Three	Three	Zero	One	Two
Experimental specific surface area ($m^2 g^{-1}$)	$\sim$10-20	20-160	80-90	$\sim$1300	$\sim$1500
Density (g cm^{-3})	2.09-2.23	3.5-3.53	1.72	>1	>1
Optical properties	Uniaxial	Isotropic	Non-linear optical response	Structure-dependent properties	97.7% of optical transmittance
Thermal conductivity (W $m^{-1} K^{-1}$)	1500-2000[a], 5-10[c]	900-2320	0.4	3500	4840-5300
Hardness	High	Ultrahigh	High	High	Highest (single layer)
Tenacity	Flexible non-elastic	-	Elastic	Flexible elastic	Flexible elastic
Electronic properties	Electrical conductor	Insulator, semiconductor	Insulator	Metallic and semiconducting	Semimetal, zero-gap semiconductor
Electrical conductivity (S cm^{-1})	Anisotropic, $2\text{-}3 \times 10^4$[a], 6[b]	-	10^{-10}	Structure-dependent	2000

[a] a-direction.
[b] c-direction.

Author's personal copy

(ii) Epitaxial growth of graphene on SiC [14,15] and metal (Ru, Pt) [16] single-crystal substrates at high temperature and in ultrahigh vacuum. It can grow large-size and high-quality graphene, but requires high-vacuum conditions, high-cost fabrication systems and suffers from the difficulty in transferring the graphene from the substrates as well as low yield.

(iii) Thermal- or plasma-enhanced chemical vapor deposition (CVD) of graphene from the decomposition of hydrocarbons at high temperatures on metal substrates (such as Ni, Cu, Pt) or metal oxide (Al_2O_3, MgO) particles. It allows for fast, uniform, large-area, high-quality graphene production, but its disadvantages are high-cost and relatively low yield. However, this strategy has great potential for further improvement [17–19].

(iv) Chemical exfoliation of graphitic materials. It involves oxidation, intercalation, exfoliation and/or reduction of graphene derivatives [20–23], such as graphite, graphite oxide, expandable graphite, CNTs, graphite fluoride and graphite intercalation compounds. It can potentially afford a bulk quantity of graphene, especially, from graphite oxide. The exfoliation and reduction of graphite oxide has now been demonstrated to be a primary low-cost strategy that can yield a large quantity of reduced graphene oxide (GO) with high processability.

(v) A bottom-up synthesis strategy from organic compounds. It is used to synthesize nano/micrographene and graphene-based materials from structurally defined precursors, such as polycyclic aromatic hydrocarbons. This approach can precisely control the formation of molecular graphene (<5 nm), nanographene (5–500 nm) and integrated macrographene (>500 nm) with well-defined structures and high processability. However, it suffers from the drawback of low productivity [24,25].

(vi) Other methods such as electrochemical exfoliation of graphite [26], graphene growth from solid state carbon [27], direct arc discharge of graphite [28], reduction of ethanol by sodium metal [29], and the thermal splitting of SiC granules [30]. Each method has its merits and shortcomings in terms of both scalability of the method and the quality of the graphene produced. Detailed discussion can be found in several excellent reviews [13,31,32].

It should be emphasized that, currently, only the chemical exfoliation method is considered as a common route toward the production of graphene at low cost and in a large quantity [20]. It first involves the oxidation of well-stacked graphite to graphite oxide [33], and is then followed by chemical reduction of GO to obtain reduced GO (rGO) [34] or thermal exfoliation of graphite oxide [35–38] to produce graphene. Generally, oxidation results in an increase of the *d*-spacing and intercalation between adjacent graphene layers, and thus weakens the interaction between adjacent sheets, and finally leads to the delamination of GO in an aqueous solution. Reduction using chemical compounds such as NH_2NH_2 [34], KOH [39], $NaBH_4$ [40], HI [41] or thermal exfoliation of graphite oxide [35–38] is commonly performed to obtain graphene from GO. For example, Schniepp et al. proposed a thermal exfoliation method to produce graphene nanosheets (GNS), where a rapid heating process is involved to exfoliate graphite oxide by quickly moving it into a furnace preheated to a high temperature [35]. Wu et al. proposed a controllable oxidation and rapid heating exfoliation strategy to tune the number of graphene layers produced by selecting a suitable starting graphite [37]. It is found that the higher the heating rate, the greater both the exfoliation and de-oxygenation degrees of graphite oxide. High annealing temperature is essential to remove structural defects. Therefore, Wu et al. developed a hydrogen arc discharge exfoliation method (>2000 °C) for the synthesis of high-quality GNS from graphite oxide with excellent electrical conductivity ($\sim 2 \times 10^3$ S cm^{-1}) and good thermal stability ($\sim$601 °C). Complete exfoliation and considerable de-oxygenation of graphite oxide and defect elimination can be simultaneously achieved during the hydrogen arc discharge exfoliation process [38]. In addition to the easy bulk synthesis, a major advantage of both GO and rGO is the controlled attachment of oxygen species on the edges and surfaces of the graphene sheets. This enables the formation of stable GO or rGO dispersions and easy functionalization in aqueous and organic solvents [42], thus offering a variety of opportunities for the simple processing of structure-dependant functionalized graphene-based materials [43]. Future methods for the production of graphene will be focused on innovation in its low-cost, large-area, large-scale production for applications.

Versatile applications of graphene

The following main applications of graphene that take advantage of its electronic properties are expected to be major breakthroughs: (i) graphene-based electronics and optoelectronics, partially replacing conventional silicon-based electronics, because graphene has ultrafast terahertz electron mobility that gives it a very bright future for building smaller, faster, cheaper electronic devices such as ballistic transistors [44], spintronics [45], field effect transistors [46], and optoelectronics [47]. (ii) Graphene-filled polymer composites with high electrical and thermal conductivity, good mechanical strength, and low percolation threshold, which, in combination with low-cost and large-scale production, allow a variety of performance-enhanced multifunctional use in electrically conductive composites, thermal interface materials, etc. [48,49]. (iii) Large-area CVD-grown graphene that is suitable to replace indium tin oxide (ITO) as cheaper, transparent conducting electrodes in various display applications such as touch screens, which is considered to be one of the immediate applications in a few years [50,51]. Another advantage over ITO is that ITO suffers from being brittle and is incapable of bending, which does not allow it to meet the requirements for flexible devices, while graphene is a more competitive solution for flexible, transparent and processable electrodes. (iv) Graphene-based electrochemical storage energy devices such as high-performance LIBs and ECs because of their greatly improved electrochemical performance of capacity, cyclability and rate capability due to its unique 2D structure and excellent physiochemical properties [52]. (v) Recent research indicates many other potential applications in gas- [11], bio-, electrochemical, and chemical sensors [53], dye-sensitized solar cells [54], organic solar cells [55], field emission devices [56], catalysts [57] and photocatalysts [58], nanogenerators [59], hydrogen storage [60], etc. Graphene may

Author's personal copy

offer other advantageous properties that outperform those of CNT and graphite, resulting in the development of new and unexpected applications.

Detailed descriptions of the properties, synthesis and applications of graphene can be found in some recent published papers [13,31,53,61–63]. Here, we only try to provide an overview of the recent progress in graphene/metal oxide composites as advanced electrodes for high-performance LIBs and ECs, highlighting the importance of synergistic effects between graphene and metal oxides in the composites and the improvement of their electrochemical properties including high capacity/capacitance, increased rate capability, excellent cyclic stability, and high energy density and power density.

Graphene for LIBs and ECs

Performance of graphene for LIBs and ECs

Graphene has attracted intense interest in electrochemical energy storage due to its large surface area, good flexibility, good chemical and thermal stability, wide potential windows, rich surface chemistry, and extraordinary electrical, thermal and mechanical properties [61], all of which are advantageous for energy storage and conversion systems. Therefore, graphene has been explored as an electrode material in electrical energy storage devices such as LIBs and ECs just after its large-scale synthesis becomes available.

Performance of graphene in LIBs

Graphite, currently the main commercially used anode material, suffers from a limited theoretical capacity of 372 mA h g^{-1} which cannot meet the requirements of high energy capacity [64]. Therefore, efforts have been made for developing other carbonaceous materials to obtain better performance. With the emergence of high-capacity carbonaceous materials, such as CNTs [65], carbon nanofibers [66], ordered mesoporous carbon [67], and hierarchically porous carbons [68], some models to explain the excess capacity were proposed. For example, lithium species may migrate into the ''cavities'' of a material [69] and may also be adsorbed on both sides of carbon layers [70] and form Li_2 covalent molecules with extra covalent sites for lithium storage [71]. Graphene shows some unique advantages compared with graphite or CNTs in energy storage applications. For example, the theoretical specific surface area of graphene is 2620 m^2 g^{-1}, much higher than that of CNTs and graphite with values of ~1300 and 10–20 m^2 g^{-1}. The large surface areas can provide more electrochemical reaction active sites for energy storage. Another distinguished advantage of graphene is its flexibilility compared to brittle graphite, which is beneficial for constructing flexible energy storage devices [53]. Compared to the graphite, the high surface-to-volume ratio and open porous systems of graphene show great advantages in fast ion transport enabling the high rate capability, which is a bottleneck for graphite with microsize bulk lithium diffusion. The controllable surface chemical groups of graphene make it easier functionation for versatile applications compared to the graphite and CNTs. Besides, graphene shows a key advantage over CNTs in that it precludes the problem of residual metallic impurities, which are difficult to remove, thus hindering many practical applications of CNTs including energy storage [53].

Yoo and Honma et al. first reported that the specific capacity of GNS could reach 540 mA h g^{-1}, much larger than that of graphite, and found that the lithium storage properties are affected by the layer spacing between the GNS. Higher capacity (730 and 784 mA h g^{-1}, Fig. 1) could be obtained by embedding CNTs or fullerene macromolecules into graphene layers to increase the interlayer distance, which may provide additional sites for the accommodation of lithium ions [72]. Wang et al. synthesized flower-like GNS with improved lithium storage capacity and cyclic stability, and claimed that lithium ions could not only adsorb on both surfaces of the GNS, but also be stored on the edges and covalent sites [73]. Guo et al. also found that GNS exhibits a relatively high reversible capacity of 672 mA h g^{-1} and good cyclic performance, and ascribed this to the presence of a large number of functional groups and the abundance of micropores and/or defects, i.e. the lithium ions could be stored on both sides of the graphene surface [74]. High-quality GNS with fewer layers (~4 layers)

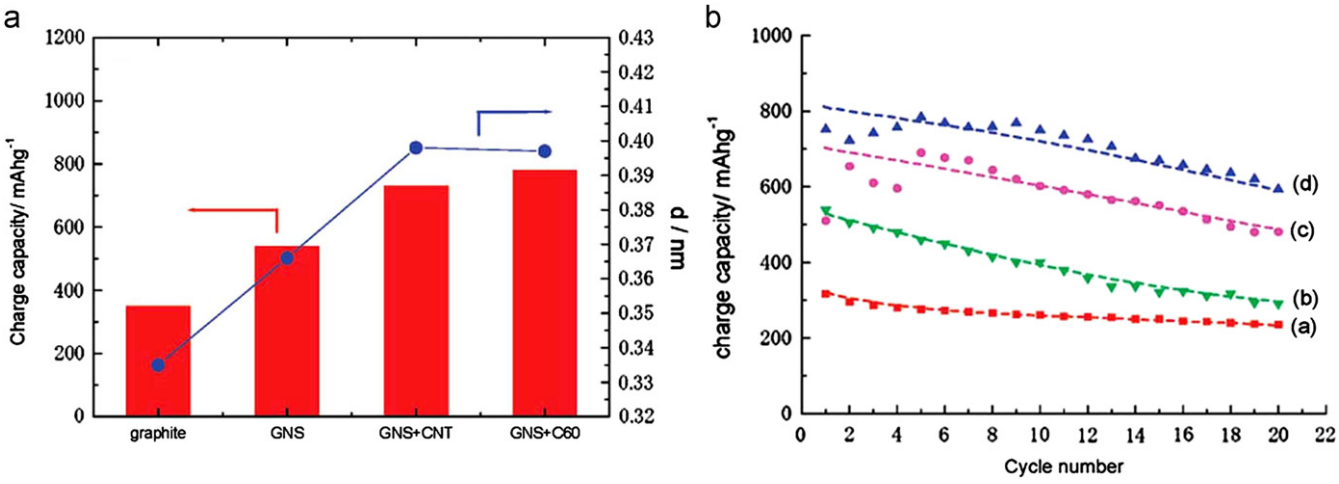

Figure 1 (a) Relationship between the *d*-spacing and the charge capacity of GNS families and graphite. (b) Charge/discharge cyclic performance of (a) graphite, (b) GNS, (c) GNS+CNT, and (d) GNS+C_{60}. Reprinted with permission [72]. Copyright 2008, American Chemical Society.

Author's personal copy

and a large specific surface area (492.5 $m^2 g^{-1}$) were reported by Lian et al., showing an initial capacity as high as 1264 mA h g^{-1} at a current density of 100 mA g^{-1}. The high capacity obtained is attributed to the fewer layers of graphene with a large surface area, curled morphology and disordered structure, many edge-type sites or nanopores, the reaction of lithium ions with the residual H, and a broad electrochemical window (0.01–3.5 V) [75]. Furthermore, Pan et al. systematically tuned the structural parameters including surface functional groups, specific surface area, interlayer spacing, defects or degree of disorder by preparing GNS using different reduction methods including hydrazine reduction, low-temperature pyrolysis, and electron beam irradiation, and investigated their effects on lithium storage properties. They found that the intensity ratio of the Raman D band to the G band is a key structural parameter for evaluating the reversible capacity and the improved lithium storage properties, and suggested that additional storage sites such as edges and defects are the dominant factors for better performance (Fig. 2) [76]. Graphene-based paper was also tested as a flexible electrode material. Although the graphene paper is mechanically strong with a Young's modulus of 41.8 GPa and tensile strength of 293.3 MPa, and shows a high electrical conductivity of 351 S cm^{-1}, its electrochemical performance is not satisfactory perhaps due to the re-stacking of GNS [77]. Recently, Wu et al. reported that nitrogen or boron doped graphene can be used as a promising large-capacity and superhigh-rate anode for high-power and high-energy lithium ion batteries under fast charge and discharge conditions [78]. It was believed that the unique two dimensional structure, disordered surface morphology, heteroatomic defects, better electrode/electrolyte wettability, increased inter-sheet distance, improved electrical conductivity and thermal stability of the doped graphene are beneficial to rapid surface Li^+ absorption and ultrafast Li^+ diffusion and electron transport [78].

Although attractive results have been achieved for GNS as electrode materials for LIBs, detailed lithium storage mechanisms are still not clear due to various possible lithium ion storage sites in a GNS electrode, such as that (1) lithium ions may intercalate few-layer GNS with a LiC_6 intercalation mechanism; (2) lithium ions may be adsorbed and accumulated on both surfaces of a GNS; (3) lithium ions may be stored on the layer edges and covalent sites; (4) lithium ions may be stored in the nanopores/cavities and defect sites; (5) lithium ions may be accommodated in the interlayer and void spaces of GNS; (6) lithium ions may react with oxygen-containing functional groups or heteroatoms such as residual hydrogen. Several reviews refer to lithium storage in carbonaceous materials and give different explanations of the extra lithium storage in GNS [31,79–83].

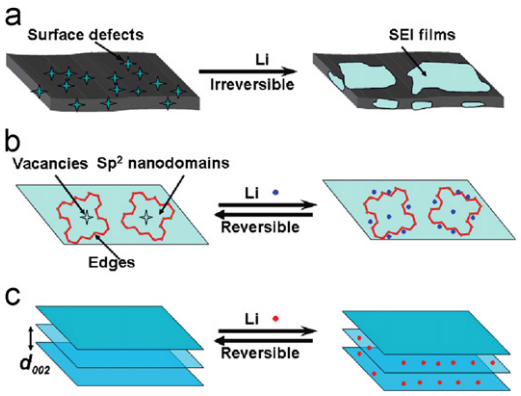

Figure 2 (a) Irreversible Li storage at the interface between GNS and electrolyte. (b) Reversible Li storage at edge sites and internal defects (vacancies, etc.) of nanodomains embedded in GNS. (c) Reversible Li storage between (002) planes. Reprinted with permission [76]. Copyright 2009, American Chemical Society.

Performance of graphene in ECs

ECs are another promising electrical energy storage device with higher energy density than conventional physical capacitors, higher charging/discharging rate capability, and longer cycle-life than primary/secondary batteries [84]. The main energy storage mechanisms include carbon-based electric double layer (EDL) and metal oxide- or polymer-based pseudo-capacitive charge storage. The former storage mode is an electrostatic (physical) process with fast charge adsorption and separation at the interface between electrode and electrolyte. The latter is a chemical process involving redox reactions between electrode materials and electrolyte ions [85]. The two charge storage modes are determined by electrode materials. Therefore, much attention has been paid to exploit electrode materials aimed at increasing specific capacitance together with high power density. In recent years, graphene has been considered a promising candidate as a supercapacitor electrode material due to its attractive characteristics such as large surface area, good flexibility, excellent electrical conductivity, good chemical and thermal stability [86], wide potential windows and abundant surface functional groups [87–90].

Two pioneer studies by Rao's and Ruoff's group show that graphene-based supercapacitors exhibit excellent performance with a specific capacitance of 75 F g^{-1} together with an energy density of 31.9 Wh kg^{-1} in ionic liquid electrolytes [87], and a specific capacitance of 135 and 99 F g^{-1} in aqueous and organic electrolytes (Fig. 3) [90]. By using a gas-solid reduction process, Wang et al. obtained reduced graphene with a low degree of agglomeration and investigated its electrochemical performance. A maximum specific capacitance of 205 F g^{-1} in an aqueous electrolyte with an energy density of 28.5 Wh kg^{-1} was obtained [88]. Lv et al. proposed a novel exfoliation approach at a very low temperature (200 °C) under high vacuum, and demonstrated that the graphene produced has a specific capacitance as high as 260 F g^{-1} at a scanning rate of 10 mV s^{-1} in an aqueous system [89]. With microwave irradiation or direct heating of GO suspensions in propylene carbonate, Zhu et al. exfoliated and reduced graphite oxide powders simultaneously. Using the rGO as electrode materials for ECs, capacitance of 191 F g^{-1} and 120 F g^{-1} was achieved in KOH and tetraethylammonium tetrafluoroborate ($TEABF_4$) electrolytes, respectively [91,92]. The tendency to restack of solvent-removed GNS makes it difficult to demonstrate the intrinsic capacitance of an individual GNS. Our work has shown that the interfacial capacitance of graphene depends on the number of layers, which can be calculated according to the specific surface area [93]. These results are attributed to the dependence of the space charge layer capacitance of graphene on the number of layers and open up the understanding of the electronic structure of multilayer graphene using an electrochemical

Author's personal copy

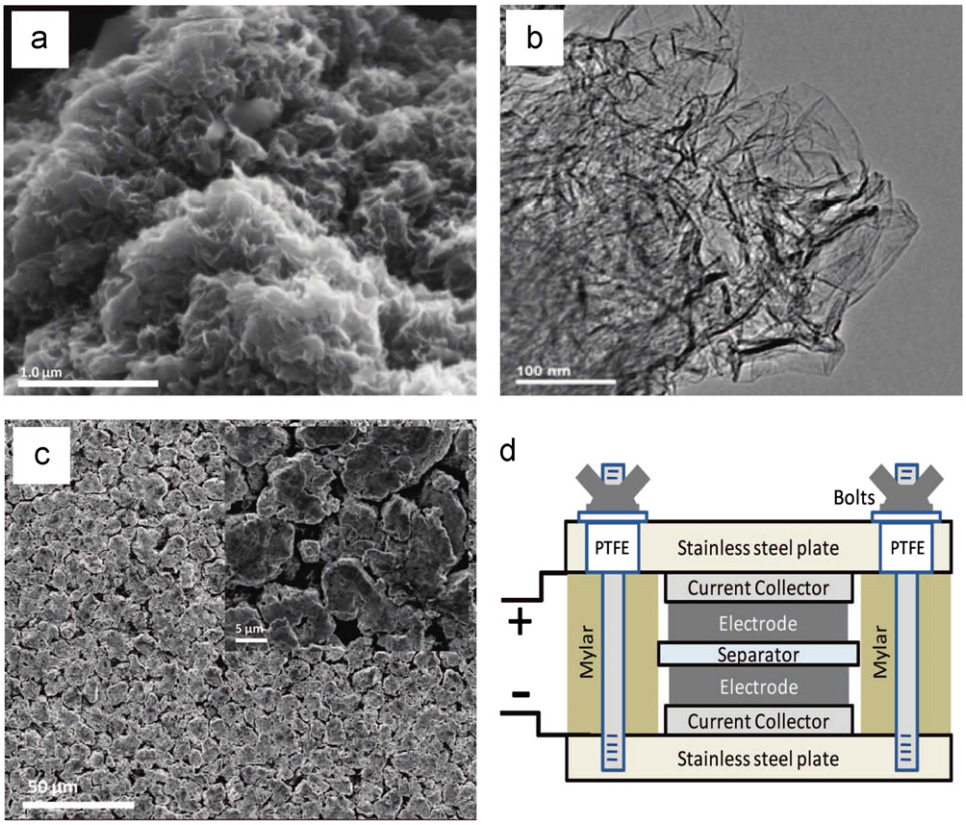

Figure 3 (a) SEM and (b) TEM images of chemically modified graphene. (c) Low and high (inset) magnification SEM images of a chemically modified graphene electrode surface. (d) Schematic of test cell assembly. Reprinted with permission [90], Copyright 2008, American Chemical Society.

approach. Recently, Tao and co-workers reported that the experimental intrinsic EDL capacitance of graphene is 21 μF cm^{-1} [94]. Liu et al. reported that a graphene-based supercapacitor exhibits an ultrahigh energy density of 85.6 Wh kg^{-1} at room temperature and 136 Wh kg^{-1} at 80 °C, both of which are comparable to a Ni metal hydride battery. These inspiring results are obtained by using environmentally benign ionic liquids which are capable of operating at high voltage of 4.5 V [95]. In another case, directly-grown vertically oriented GNS on nickel current collectors as electrodes for EDL capacitors (EDLCs) efficiently filtered 120-Hz current with a resistor-capacitor time constant less than 0.2 ms which is four orders of magnitude faster than that of a typical EDLC (~1 s, much longer than the requirement of 8.3 ms for the common application of 120 Hz filtering) [96].

Pros and cons of graphene and metal oxides in LIBs and ECs

Pros of graphene in LIBs and ECs

The above results indicate that graphene holds considerable promise as a new anode material in LIBs and ECs due to its unique physical and chemical properties including (Table 2): (1) superior electrical conductivity to graphitic carbon; (2) high surface area - the theoretical specific surface area of monolayer graphene is 2620 $m^2 g^{-1}$; (3) a high surface-to-volume ratio, which provides more active sites for ion adsorption and/or electrochemical reactions; (4) ultrathin thickness that obviously shortens the diffusion distance of ions; (5) structural flexibility that paves the way for constructing flexible electrodes; (6) thermal and chemical stability which guarantee its use in harsh environments; (7) abundant surface functional groups which make it hydrophilic in aqueous electrolytes, and provide binding sites with other atoms or functional groups; and (8) a broad electrochemical window that is critical for increasing energy density, which is proportional to the square of the window voltage. In addition, graphene electrodes used for ECs have a major innovation arising from the fact that they are not like activated carbons which achieve a large surface area because of a rigid porous structure but they have an intrinsic flexible, open pore system [61,89], which is beneficial for ion transport kinetics. This feature is also important in LIBs. Another important aspect that cannot be neglected is the cost for mass production. GNS prepared through chemical exfoliation of graphite in polar solvents or chemical reduction of GO can be produced on a large scale at a relatively low cost, which is important for their practical applications.

Cons of graphene in LIBs and ECs

The following great challenges for GNS used as electrodes in LIBs and ECs remain (Table 2): (1) lithium storage mechanisms in GNS need to be clearly clarified because different opinions exist, such as a Li_2 covalent molecule model predicting the highest Li storage capacity of 1116 mA h g^{-1} (LiC_2) [76] or absorption of lithium on both sides of a GNS

Author's personal copy

Table 2 The pros and cons of graphene, metal oxides, and graphene/metal oxide composites in LIBs and Ecs.

Pros of graphene	Cons of graphene	Pros of MO	Cons of MO	Pros of graphene/MO composites
Superior electrical conductivity	Serious agglomeration	Very large capacity/ capacitance	Poor electrical conductivity	Synergistic effects
Abundant surface functional groups	Re-stacking	High packing density	Large volume change	Suppressing the volume change of MO
Thermal and Chemical stability	Large Irreversible capacity	High energy Density	Severe aggregation/ agglomeration	Suppressing agglomeration of MO and re-stacking of graphene
Large surface area	Low initial coulombic efficiency	Rich resources	Large irreversible capacity	Uniform dispersion of MO
High surface-to-volume ratio	Fast capacity fading		Low initial coulombic efficiency	Highly conducting and flexible network
Ultrathin thickness	No clear lithium storage mechanism		Poor rate capability	High capacity/capacitance, good rate capability
Structural flexibility	No obvious voltage plateau		Poor cycling stability	Improved cycling stability
Broad electrochemical window	Large voltage hysteresis			Improved energy/power densities

MO: Metal oxides.

resulting in two layers of lithium per layer of GNS to give a Li_2C_6 model [97]. Relationships between lithium storage and defects, oxygen-containing functional groups, number of layers, and lateral size of the graphene are needed to elucidate. (2) The initial capacity of GNS is much higher than that of graphite-based ones but suffers from large irreversible capacity, low initial Coulombic efficiency, and fast capacity fading, which are mainly due to the re-stacking of GNS and side reactions between GNS and electrolytes arising from the abundant functional groups and defects. (3) There is no obvious voltage plateau to provide stable potential outputs, and there is a large hysteresis between the charge/discharge curves of GNS which will be a major drawback for their practical use in commercial LIBs. As for ECs, the EDL capacitance is limited by the easy agglomeration and re-stacking of GNS, resulting in small surface area and low energy density. (4) Although effective reduction of GO is carried out, the electrical conductivity of the resulting reduced GO is usually quite low compared to graphite.

Graphene is generally considered an ideal building block in composite materials combined with a variety of inorganic compounds, such as metal oxides, which exhibit exceptional performance in applications such as supercapacitors, batteries, sensors, photovoltaics. Therefore, significant synergistic effects are expected between graphene and inorganic components when combined at the molecular scale and these may create novel properties different from those of each individual component.

Pros and cons of metal oxides in LIBs and ECs

Due to the limited capacity of graphite, many efforts have been focused on finding substitutes with larger capacity and slightly more positive intercalation voltage compared to Li/Li^+, so as to reduce the possible safety problems of lithium plating [98]. Metal oxides, typically providing a capacity more than two times larger than that of graphite with higher potential, have aroused wide interest [99]. The electrode reaction mechanism of metal oxides can be typically classified into three groups [100–102]: (1) conversion reaction, (2) Li-alloy reaction, and (3) Li insertion/extraction reaction. The conversion reaction mechanism is as follows:

$$M_xO_y + 2ye^- + 2yLi^+ \leftrightarrow x[M]^0 + yLi_2O$$

where M is a metal such as Sn, Co, Ni, Fe, Cu, and Mn, and the final product consists of a homogeneous distribution of metal nanoparticles embedded in a Li_2O matrix. However, their application in practical LIBs is significantly hindered by the poor cyclic performance arising from huge volume expansion and severe aggregation of metal oxides during charge/discharge. Another drawback is the large voltage hysteresis between charge and discharge together with poor energy efficiency. The Li-alloy reaction mechanism is as follows:

$$M_xO_y + 2ye^- + 2yLi^+ \rightarrow x[M]^0 + yLi_2O$$

$$M + ze^- + zLi^+ \leftrightarrow Li_zM$$

For example, a tin-based oxide first follows the conversion reaction mentioned above forming Li_2O and metallic tin, subsequently, the *in-situ* formed tin distributed in Li_2O can store and release lithium ions according to Li–Sn alloying/de-alloying reactions up to the theoretical limit of $Li_{4.4}Sn$ corresponding to a theoretical reversible capacity of 782 mA h g^{-1} based on the mass of SnO_2 [100]. However, its poor cyclic performance caused by large volume changes (up to 300%) during charge/discharge leads to mechanical disintegration and the loss of electrical connection of the active material from current collectors. Li insertion/extraction reaction mechanism involves the insertion and extraction of Li^+ into and from the lattice of the metal oxide which can be described as follows:

$$MO_x + ye^- + yLi^+ \leftrightarrow Li_yMO_x$$

For instance, TiO_2 is a common anode metal oxide follows a typical Li intercalation process with a volume change

Author's personal copy

smaller than 4% in the reaction: $TiO_2 + xLi^+ + xe^- \leftrightarrow 4Li_xTiO_2$ ($0 \leq x \leq 1$). The lithium intercalation and extraction process with a small lattice change ensures its structural stability and cycling life. The lithium intercalation potential is about 1.5 V, thus intrinsically maintaining the safety of the electrode through the avoidance of electrochemical Li deposition. However, its drawback is low specific capacity, poor lithium ionic and electronic conductivity and high polarization, resulting from the slow ionic and electronic diffusion of bulk TiO_2 [100]. In supercapacitors, metal oxides provide higher pseudo-capacitance through bulk redox reactions compared with surface charge storage of carbonaceous materials. However, the large volume variation induced structure change breaks the stability of electrode materials, causing the rapid capacity loss during charge/discharge processes. Lithium can react with metallic/semimetallic elements and metal alloys, such as Si, Sn, Ge, Bi, Cu–Sn, and Ni–Sn showing high capacity, while their applications are facing the same challenge as metal oxides of large volume change during Li alloying/dealloying processes, which leads to the severe capacity fading [100–102]. These advantages and disadvantages of metal oxides for energy storage are also presented in Table 2.

Graphene/metal oxide composites in LIBs and ECs

Structural models of graphene/metal oxide composites

As described above, one of the intractable issues for the use of graphene in LIBs and ECs is that chemically derived graphene generally suffers from serious agglomeration and re-stacking after removal of dispersed solutions and drying due to the van der Waals interactions between GNS, consequently lowering the electrochemical performance of GNS in LIBs and ECs.

To fully use all the potential advantages of graphene in LIBs and ECs, fabrication of graphene/metal oxide composites is expected to be an effective and practical method (Fig. 4). The aim is to maximize the practical use of the combined advantages of both graphene and metal oxides as active materials for improving the electrochemical energy storage, and to lower or even solve the current electrode problems of the individual components of graphene or metal oxides as active materials. In a composite, graphene provides chemical functionality and compatibility to allow easy processing of metal oxides in the composite. The metal oxide component mainly provides high capacity depending on its structure, size and crystallinity. The resultant composite is not merely the sum of the individual components, but rather a new material with new functionalities and properties. From the viewpoint of structure, on one hand, metal oxides anchored or dispersed on GNS not only suppress the agglomeration and re-stacking of GNS but also increase the available surface area of the GNS alone, leading to high electrochemical activity. On the other hand, GNS as a support of metal oxides can induce the nucleation, growth and formation of fine metal oxide nano-/microstructures with uniform dispersion and controlled morphology on the surface of graphene with high chemical functionality. The final metal oxide-anchored graphene and the graphene-supported metal oxide can form a perfect integrated structure with a developed electron conductive network and shortened ion transport paths. Significant synergistic effects often occur in graphene/metal oxide composites because of size effects and interfacial interactions.

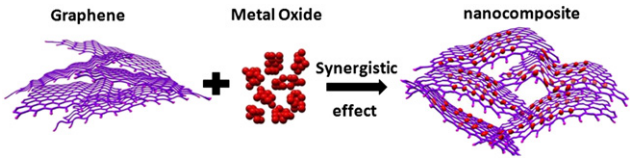

Figure 4 Schematic of the preparation of graphene/metal oxide composites with synergistic effects between graphene and metal oxides.

Several structural models of graphene/metal oxide composites are already proposed (Fig. 5): (a) nano-sized oxides anchoring on graphene for LIBs (SnO_2 [103–116], Co_3O_4 [117–123], Fe_2O_3 [124,125], Mn_3O_4 [126], MnO [127], Fe_3O_4 [128–134], NiO [135], MoO_3 [136], TiO_2 [137–139], CuO [140–142], Cu_2O [143,144], $LiFePO_4$ [138,145], CeO_2 [146] etc.), and ECs (SnO_2 [104], Co_3O_4 [147,148], RuO_2 [149,150], TiO_2 [150], MnO_2 [78,151–158], Mn_3O_4 [159], ZnO [160,161], Fe_3O_4 [150] etc); (b) graphene-wrapped metal oxide particles (Fe_3O_4 [162], TiO_2 [163], NiO [164], MoO_2 [165], V_2O_5 [166], etc.); (c) graphene-encapsulated metal oxides for LIBs (Co_3O_4 [167], Fe_3O_4 [168,169], Fe_2O_3 [125], etc.); (d) a 2D sandwich-like model [170–172]: graphene as a template for the creation of a metal oxide/GNS sandwich-like structure (such as Co_3O_4 [170], TiO_2 [172]); (e) graphene/metal oxide layered composites composed of aligned layers of metal oxide (SnO_2–NiO–MnO_2 [173], TiO_2 [174], NiO [175], MnO_2 [176,177], etc.)-anchored graphene; (f) 3D graphene (normally $\leq$10 wt% in composite) conductive networks among metal oxides ($Li_4Ti_5O_{12}$ [178,179], $LiFePO_4$ [149], TiO_2 [180], $Li_3V_2(PO_4)_3$ [181], Fe_2O_3 [182], etc.). These composite materials and their electrochemical properties in LIBs and ECs are listed in Table 3. The functions and synergistic effects of graphene and metal oxides in graphene/metal oxide composites can be briefly summarized (Table 2): (1) graphene as a 2D support for uniformly anchoring or dispersing metal oxides with well-defined sizes, shapes and crystallinity; (2) metal oxides suppressing the re-stacking of graphene; (3) graphene acting as a 2D conductive template or building a 3D conductive porous network for improving the poor electrical properties and charge transfer pathways of pure oxides; (4) graphene suppressing the volume change and agglomeration of metal oxides; (5) oxygen-containing groups on graphene ensures good bonding, interfacial interactions and electrical contacts between graphene and metal oxides.

Multifunctionalities of graphene as a support

Graphene as a 2D support

It has been demonstrated that graphene or reduced GO can serve as a perfect 2D support for anchoring metal or metal oxide nanoparticles [57,184]. Nanomaterials are of great scientific interest due to their size-related unique properties and a wide variety of potential applications. However, a common phenomenon of metal oxides during preparation is uncontrolled agglomeration and growth of large particles

Author's personal copy

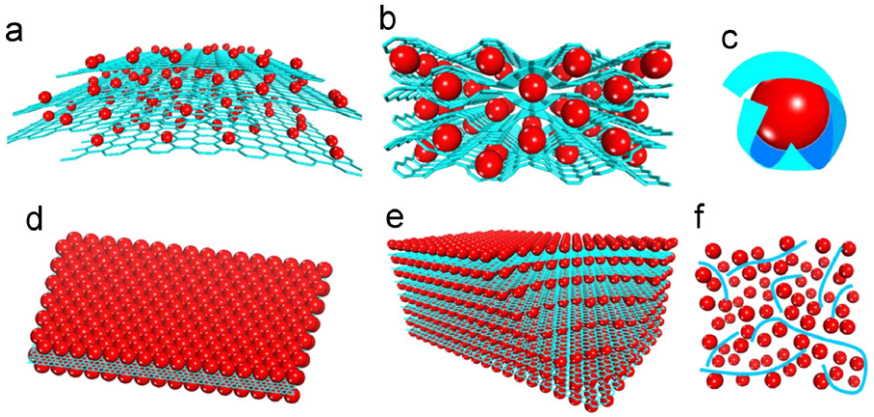

Figure 5 Schematic of structural models of graphene/metal oxide composites: (a) Anchored model: nanosized oxide particles are anchored on the surface of graphene. (b) Wrapped model: metal oxide particles are wrapped by graphene. (c) Encapsulated model: oxide particles are encapsulated by graphene. (d) Sandwich-like model: graphene serves as a template for the creation of a metal oxide/graphene/metal oxide sandwich-like structure. (e) Layered model: a structure composed of alternating layers of metal oxide nanoparticles and graphene. (f) Mixed model: graphene and metal oxide particles are mechanically mixed and graphene forms a conductive network among the metal oxide particles. Red: metal oxide particles; Blue: graphene sheets.

Table 3 Examples of structures and electrochemical properties of the graphene/metal oxide composites for LIBs and ECs reported in the literatures.

Structural model	G/MO	LIBs/ ECs	MO morphology	Performance improvements	Refs.
Anchored	G/SnO_2	LIBs	NPs	A specific capacity of 810 mA h g^{-1}, 70% capacity retention after 30 cycles	[103]
	G/SnO_2	LIBs	NPs	A specific capacity of 765 mA h g^{-1} in the first cycle, maintained a capacity of 520 mA h g^{-1}after 100 cycles	[104]
	G/SnO_2	LIBs	NPs	A reversible capacity of 862 mA h g^{-1}, maintained 665 mA h g^{-1} after 50 cycles	[105]
	G/SnO_2	LIBs	NPs	An initial reversible capacity of 786 mA h g^{-1}, 71% capacity retention after 50 cycles	[106]
	G/SnO_2	LIBs	Echinoid-like NPs	A reversible capacity of 634 mA h g^{-1} with a coulombic efficiency of 98% after 50 cycles	[107]
	G/SnO_2	LIBs	NPs	The capacities were 673, 424, 295, 190 and 120 mA h g^{-1} at 130, 450, 1400, 6000 and 8000 mA g^{-1}, respectively	[108]
	G/SnO_2	LIBs	NPs	600 mA h g^{-1} after 50 cycles and 550 mA h g^{-1} after 100 cycles, 550 mA h g^{-1}at the 2 C rate, and 460 mA h g^{-1} at as high rate as 5 C rate	[109]
	G/SnO_2	LIBs	Nanorods	A reversible capacity of 838 mA h g^{-1}, the charge capacity of the hybrid electrode remains at 510 mA h g^{-1} after 20 cycles	[110]
	G/SnO_2	LIBs	NPs	A reversible specific capacity of 1304 mA h g^{-1} at 100 mA g^{-1} and the reversible capacity was still as high as 748 mA h g^{-1} at 1000 mA g^{-1}	[111]
	G/SnO_2	LIBs	NPs	A charge capacity of 840 mA h g^{-1} (with capacity retention of 86%) after 30 cycles at 67 mA g^{-1}, and it could retain a charge capacity of about 590 mA h g^{-1} at 400 mA $g^{-1}$and 270 mA h g^{-1} at 1000 mA g^{-1} after 50 cycles	[112]
	G/SnO_2	LIBs	Nanosheets	A reversible capacity of 518 mA h g^{-1} after 50 cycles at 400 mA g^{-1}	[113]
	G/SnO_2	LIBs	Particles	A capacity of 2140 mA h g^{-1} and 1080 mA h g^{-1} for the first discharge and chargeat a current density of 50 mA h g^{-1}, and good capacity retention with a capacity of 649 mA h g^{-1} after 30 cycles	[114]
	G/SnO_2	LIBs	NPs	A stable capacity of 775.3 mA h g^{-1} after 50 cycles at 100 mA g^{-1}	[115]
	G-CNT/ SnO_2	LIBs	NPs	The capacities of 345 and 635 mA h g^{-1} can be obtained at 1.5 and 0.25 A g^{-1} and the flexible SnO_2-G-CNT papers present a stable capacity of 387 mA h g^{-1} at 0.1 A g^{-1} after 50 cycles	[116]
	G/Co_3O_4	LIBs	NPs	Large reversible capacity (935 mA h g^{-1} after 30 cycles), excellent cyclic performance, good rate capability	[117]

Author's personal copy

Table 3 (*continued*)

Structural model	G/MO	LIBs/ ECs	MO morphology	Performance improvements	Refs.
	G/Co_3O_4	LIBs	Nanosheets	A high capacity of 931 mA h g^{-1} was obtained at 4450 mA g^{-1}	[118]
	G/Co_3O_4	LIBs	Rods	Reversible capacity after 100 cycles is 975 mA h g^{-1} with the irreversible capacity loss less than 3%	[119]
	G/Co_3O_4	LIBs	NPs	$>$800 mA h g^{-1} reversibly at 200 mA g^{-1}, $>$550 mA h g^{-1} at 1000 mA g^{-1}	[120]
	G/Co_3O_4	LIBs	NPs	941 mA h g^{-1} in the initial cycle at a current density of 200 mA g^{-1} and an excellent cyclic performance of 740 mA h g^{-1} after 60 cycles	[121]
	G/Co_3O_4	LIBs	Nanowall	A capacity of 732 mA h g^{-1} can be obtained after 100 cycles at 150 mA g^{-1}	[122]
	G/Co_3O_4	LIBs	NPs	An initial reversible lithium storage capacity of 722 mA h g^{-1} in LIBs and a specific capacitance of 478 F g^{-1} in 2 M KOH	[123]
	G/Fe_2O_3	LIBs	NPs	The first discharge and charge capacities are 1693 and 1227 mA h g^{-1} at 100 mA g^{-1} and retain a reversible capacity of 1027 mA h g^{-1} after 50 cycles	[124]
	G/Fe_2O_3	LIBs	Nanowires, NPs	The initial discharge capacity is 1338 mA h g^{-1} and 58% of the reversible capacity can be maintained over 100 cycles at 200 mA g^{-1}	[125]
	G/Co_3O_4	ECs	Scroll	A specific capacitance of 163.8 F g^{-1} and still remained ~140 F g^{-1} up to 10 A g^{-1}, and 93% retention after 1000 cycles at 20 mV s^{-1}	[147]
	G/Co_3O_4	ECs	NPs	A maximum specific capacitance of 243.2 F g^{-1} at a scan rate of 10 mV s^{-1}, 95.6% specific capacitance retained after 2000 cycle tests	[148]
	G/RuO_2	ECs	NPs	High specific capacitance (570 F g^{-1}), enhanced rate capability, excellent lectrochemical stability (97.9% retention after 1000 cycles), and high energy density (20.1 Wh kg^{-1}) at low rate (100 mA g^{-1}) or high power density (10,000 W kg^{-1}) at a reasonable energy density (4.3 Wh kg^{-1})	[149]
	$G/RuO_2G/TiO_2G/Fe_3O_4$	ECs	NPs	A maximum specific capacitance of 265, 60, and 180 F g^{-1} are obtained at the sweep rate of 10 mV/s for RuO_2/G, TiO_2/G, and Fe_3O_4/G, respectively	[150]
	G/MnO_2	ECs	Needle-like nanocrystals	A capacitance of 216.0, 197.2, 141.5, and 111.1 F g^{-1} at 150, 200, 500, and 1000 mA g^{-1}, retained ~84.1% of initial capacitance after 1000 cycles	[151]
	G/MnO_2	ECs	Particles	Specific capacitance of 310 F g^{-1} at 2 mV s^{-1} (even 228 F g^{-1} at 500 mV s^{-1}), 88% capacitance retention at 100 mV s^{-1} and 74% capacitance retention at 500 mV s^{-1}	[183]
	G/MnO_2	ECs	Nanowires	A superior energy density of 30.4 Wh kg^{-1}, high power density (5000 W kg^{-1} at 7.0 Wh kg^{-1})	[152]
	G/MnO_2	ECs	Nanosheet	A specific capacitance of 188 F g^{-1} was achieved at 0.25 A g^{-1}, the capacitive retention was about 89% after 1000 cycles	[153]
	G/MnO_2	ECs	NPs	A high specific capacitance of 324 F g^{-1} achieved at 10 mV s^{-1}, excellent long-term cycle stability (only 3.2% capacitance loss after 1000 cycles)	[154]
	G/MnO_2	ECs	Flower-like	328 F g^{-1} at the charging current of 1 mA with an energy density of 11.4 Wh kg^{-1} and 25.8 kW kg^{-1} of power density	[155]
	G/MnO_2	ECs	NPs	A specific capacitance of 308.5 F g^{-1} at 5 mV s^{-1} and the capacitance retained nearly 100% of the initial capacitance after 500 cycles	[156]
	G/MnO_2	ECs	Nanoflower	315 F g^{-1} was achieved and a maximum power density of 110 kW kg^{-1}, an energy density of 12.5 Wh kg^{-1} as well as excellent cycling performance of 95% capacitance retention over 5000 cycles	[157]
	G/MnO_2	ECs	Nanofibre	113.5 F g^{-1} at a scan rate of 1 mV s^{-1} with maximum energy density of 51.1 Wh kg^{-1} and 97% specific capacitance retained after 1000 cycles	[158]
	G/Mn_3O_4	LIBs	NPs	A high specific capacity up to 900 mA h g^{-1}, good rate capability and cycling stability	[126]
	G/Mn_3O_4	ECs	NPs	A high specific capacitance of 175 F g^{-1} in 1M Na_2SO_4 electrolyte and 256 F g^{-1} in 6M KOH electrolyte	[159]
	G/MnO	LIBs	NPs	A reversible capacity of 635 mA h g^{-1} at 0.2 C and the rate capacity retention 5 C/0.2 C $>$ 70%	[127]

Author's personal copy

Table 3 (*continued*)

Structural model	G/MO	LIBs/ ECs	MO morphology	Performance improvements	Refs.
	G/Fe_3O_4	LIBs	NPs	A large reversible specific capacity of 1048 mA h g^{-1}at the 90th cycle, enhanced cycling performances (about 650 mA h g^{-1} after 50 cycles) and high rate capabilities (350 mA h g^{-1} at 5 C)	[128]
	G/Fe_3O_4	LIBs	NPs	A specific capacity of 1280 mA h g^{-1} at 0.1 C cycling and 860 mA h g^{-1} at 4 C rate with exceptional stability	[129]
	G/Fe_3O_4	LIBs	NPs	A reversible capacity of 474 mA h g^{-1} at a current density of 1600 mA g^{-1}; a capacity of 637 mA h g^{-1} at 200 mA g^{-1} was retained after 60 cycles	[130]
	G/Fe_3O_4	LIBs	NPs	The capacity keeps at 796 mA h g^{-1} after 200 cycles without any fading, and the reversible capacity attains ~550 mA h g^{-1} and 97% of initial capacity is maintained after 300 cycles at 1 A g^{-1}	[131]
	G/Fe_3O_4	LIBs	NPs	A high reversible capacity is about two and a half times higher than that of graphite-based anodes at a 0.05 C rate, and an enhanced reversible capacity of about 200 mA h g^{-1} even at a high rate of 10 C (9260 mA g^{-1})	[156]
	G/Fe_3O_4	LIBs	NPs	The reversible capacity is 538.7 mA h g^{-1} after 50 cycles	[133]
	G/Fe_3O_4	LIBs	NPs	A specific discharge capacity of 952.0 mA h g^{-1} in the initial cycle and 842.7 mA h g^{-1} after 100 cycles.	[158]
	G/NiO	LIBs	NPs	A capacity of 450 mA h g^{-1} after 100 cycles at 1 C (1 C = 300 mA g^{-1}) and a discharge capacitiy of 185 mA h g^{-1} at 20 C	[135]
	G/MoO_3	ECs	NPs	Specific capacitance of 86.3 F g^{-1} was obtained at 100 mA g^{-1} and retained about 92.7% (80 F g^{-1}) of initial capacitance after 100 cycles	[136]
	G/TiO_2	LIBs	Rodlike	87 mA h g^{-1} at a rate of 30 C (2 min of charging or discharging)	[137]
	G/TiO_2	LIBs	Particles	Negligible fade after 700 cycles at 1 C rate with columbic efficiency reaching 100% over the entire cycling test except for the initial few cycles	[138]
	G/TiO_2	LIBs	Nanosheets	A reversible capacity of 161 mA h g^{-1} can be retained at 1 C after 120 charge-discharge cycles and delivered a capacity of 125 mA h g^{-1} and 107 mA h g^{-1} at 5 C and 20 C, respectively	[139]
	G/ZnO	ECs	Particles	A specific capacitance of 11.3 F g^{-1} with better reversible charging/ discharging ability	[160]
	G/ZnO	ECs	Particles	A large capacitance (62.2 F g^{-1}), excellent cyclic performance, and maximum power density (8.1 kW/kg)	[161]
	G/CuO	LIBs	Urchin-like	Reversible capacity of 600 mA h g^{-1} at 65 mA g^{-1} after100 discharge-charge cycles	[140]
	G/CuO	LIBs	NPs	A reversible capacity of 583.5 mA h g^{-1} with 75.5% retention of the reversible capacity after 50 cycles	[141]
	G/CuO	LIBs	Hollow NPs	The reversible capacity attains 640 mA h g^{-1} at 50 mA g^{-1} and the capacity retention is ca. 96%. At 1 A g^{-1}, the reversible capacity reaches 485 mA h g^{-1} and remains at 281 mA h g^{-1} after 500 cycles	[142]
	G/Cu_2O	LIBs	Particles	1100 mA h g^{-1} in the first cycle	[143]
	G/Cu_2O	ECs	NPs	An averaged capacity values of 31.0, 26.0, and 24.0 F g^{-1} at 100, 200, and 400 mA g^{-1}; a good cycling behavior with no obvious loss during 5000 cycles with the retention coefficient of 72.7% of initial capacitance	[144]
	G/CeO_2	LIBs	Particles	A specific capacity of 605 mA h g^{-1} at the 100^{th} cycle at 50 mA g^{-1} and the capacities of 414, 320, 222 and 146 mA h g^{-1} could be obtained at 100, 200, 400 and 800 mA g^{-1}, respectively	[146]
Wrapped	G/Fe_3O_4	LIBs	Particles	A high reversible specific capacity approaching 1026 mA h g^{-1} after 30 cycles at 35 mA g^{-1} and 580 mA h g^{-1} after 100 cycles at 700 mA g^{-1} as well as improved cyclic stability and excellent rate capability	[162]
	G/TiO_2	LIBs	Hollow particles	A reversible capacity of 90 mA h g^{-1} can be delivered at a current rate of 10 C with good cyclic retention up to 180 cycles	[163]
	G/NiO	ECs	NPs	A capacitance of 150-220 F g^{-1} at 100 mA g^{-1} and the capacity stays at 130 F g^{-1} with cycling to 1000 cycles at a current density of 2 A g^{-1}	[164]

Author's personal copy

Table 3 (*continued*)

Structural model	G/MO	LIBs/ ECs	MO morphology	Performance improvements	Refs.
	G/MoO_2	LIBs	Rodlike	The initial discharge and charge capacities are 468.2 and 342.0 mA h g^{-1} and the capacity reaches 407.7 mA h g^{-1} after 70 cycles at 2000 mA g^{-1}	[165]
	G/V_2O_5	LIBs	Nanowire	An initial specific discharge capacity of 412 mA h g^{-1} at 50 mA g^{-1} and a capacity of 316 mA h g^{-1} at the current density of 1600 mA g^{-1}	[166]
Encapsulated	G/Co_3O_4	LIBs	NPs	High reversible capacity of 1100 mA h g^{-1} in the first 10 cycles, over 1000 mA h g^{-1} after 130 cycles, with excellent cycle performance	[167]
	G/Fe_3O_4	LIBs	NPs	A stable capacity of 650 mA h g^{-1} with no noticeable fading for 100 cycles	[168]
	G/Fe_3O_4	LIBs	Hollow NPs	A stable high specific reversible capacity of around 900 mA h g^{-1} which was nearly unvarying over 50 cycles	[169]
2D sandwich	G/Co_3O_4	LIBs	Nanosheets	A first reversible capacity of 915 mA h g^{-1} at C/5, and 84% capacity retention after 30 cycles	[170]
	G/TiO_2	LIBs	Nanosheets	A first discharge capacity of 269 mA h g^{-1} is achieved at 0.2 C and a capacity of 202 mA h g^{-1} in the charging process, the reversible capacities are retained at 162 and 123 mA h g^{-1} at 1 C and 10 C	[172]
Layered	G/SnO_2; G/NiO; G/MnO_2	LIBs	NPs	Specific capacity of 625, 550, 225 mA h g^{-1} are obtained at 0.01, 0.02 and 0.08 A g^{-1} for SnO_2-graphene; the capacity of the NiO-graphene composite is stable upon lithiation/delithiation over 100 cycles	[173]
	G/TiO_2 at TiO_xN_y/TiN	LIBs	Nanospindles	The specific capacity was 175, 166, 150 and 130 mA h g^{-1} at a rate of C/3, 1 C, 3 C and 12 C, respectively	[174]
	G/NiO	LIBs	Nanosheets	A large initial charge capacity of 1056 mA h g^{-1} at 0.1 C and retained 1031 mA h g^{-1} after 40 cycles; the charge capacities of 872, 657, and 492 mA h g^{-1} were obtained at 718, 1436 and 3590 mA g^{-1}, respectively	[175]
	G/MnO_2	LIBs	Nanotube	A reversible specific capacity of 495 mA h g^{-1} at 100 mA g^{-1} after 40 cycles and reached a capacity of 208 mA h g^{-1} at1600 mA g^{-1}	[176]
	G/MnO_2	LIBs	Rodlike	A discharge capacity of 1105 mA h g^{-1} was observed on the second cycle, remaining 948 mA h g^{-1} after 15 cycles; a reversible capacity of 930, 836, and 698 mA h g^{-1} at 100, 200, and 400 mA g^{-1}, respectively	[177]
Mixed	G/$Li_4Ti_5O_{12}$	LIBs	Fibrous like	Specific capacities were 164 mA h g^{-1} at 0.2 C and 137 mA h g^{-1} at 8 C	[178]
	G/$Li_4Ti_5O_{12}$	LIBs	NPs	A specific capacity of 122 mA h g^{-1} even at a very high charge/discharge rate of 30 C	[179]
	G/$LiFePO_4$	LIBs	Particles	A discharge capacity of 160.3 mA h g^{-1} at 0.1 C and 81.5 mA h g^{-1} at 10 C	[149]
	G/TiO_2	LIBs	Sphere	Specific capacity at the rate of 50 C is as high as 97 mA h g^{-1}	[180]
	G/$Li_3V_2(PO_4)_3$	LIBs	NPs	The specific capacities are 118 mA h g^{-1} and 109 mA h g^{-1} at 5 C and 20 C discharge rates, and 82 mA h g^{-1} at a higher current rate of 50 C, reaching 64% of the initial charge capacity at 0.1 C	[181]
	G/Fe_2O_3	LIBs	Spherical particles	A high discharge capacity of 660 mA h g^{-1} during up to 100 cycles at the current density of 160 mA g^{-1} and capacities of 702, 512, 463 and 322 mA h g^{-1} at 400, 800, 1600 and 2400 mA g^{-1}, respectively	[182]

G: Graphene; MO: Metal oxides; NPs: Nanoparticles.

that often lose their dispersibility and good properties. It is well known that a bulk material has physical properties regardless of its size, which differs significantly from nanomaterials for which size-dependent properties are observed. Therefore, synthesis of metal oxide nanostructures with controlled size, uniform morphology, good crystallinity and high dispersion remains a major challenge. Recent advances suggest that reduced GO is a good 2D support to nucleate and anchor metal oxide nanoparticles on the edges and surface [57,184]. General wet-chemistry strategies, such as chemical *in-situ* deposition, sol-gel processes, and hydrothermal synthesis, are widely used in the fabrication of a broad range of graphene/metal oxide composites starting from a dispersed solution of suspended graphene which acts as a 2D precursor for an integrated support network for discrete metal nanoparticles (Fig. 6). First, both GO and reduced GO are dispersed in aqueous or organic solvents by electrostatic stabilization and chemical functionalization. The presence of

Author's personal copy

hydrophilic oxygen-containing functional groups such as epoxides, hydroxides, and carboxylic groups on the surface enables GO or reduced GO to be well dispersed. Such dispersions are a good template suspension for chemical reaction with metal ions from the precursors of inorganic and organic metal salts, which undergo hydrolysis or *in situ* redox reactions to anchor them on the surface of graphene with rich functionalities, followed by annealing. Special emphasis is given to the important role of graphene that can suppress the agglomeration of metal oxide nanoparticles. For example, research under the same experimental conditions have shown that small RuO_2 nanparticles with a size of 5–20 nm are homogeneously anchored on the surface of graphene (Fig. 7a) [149]. In sharp contrast, without the presence of graphene, the as-prepared hydrous RuO_2 powder tends to spontaneously agglomerate and form big particles with a size of hundreds of nanometers even to tens of micrometers (Fig. 7b) [149], and similar behavior is observed for Co_3O_4 (Fig. 7c and d) [117]. This intriguing phenomenon observed during the preparation process suggests the presence of a strong synergistic effect between graphene and metal oxides. We here stress that this wet-chemistry strategy is used primarily for the fabrication of graphene/metal oxide multifunctional materials for applications in LIBs and ECs. It provides a simple and practical way to obtain a uniform distribution of metal oxide nanoparticles on graphene (or GO) with controllable size, shape and crystallinity. Wang et al. used anionic sulfate surfactants to assist the stabilization of graphene in aqueous solutions and facilitate the self-assembly of *in-situ* grown

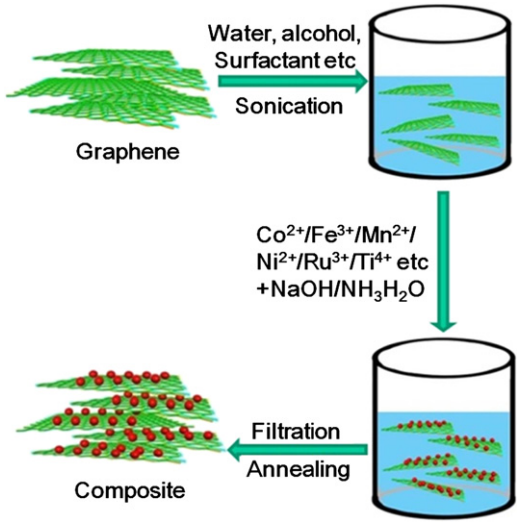

Figure 6 A general wet-chemistry strategy to fabricate graphene/metal oxide composites.

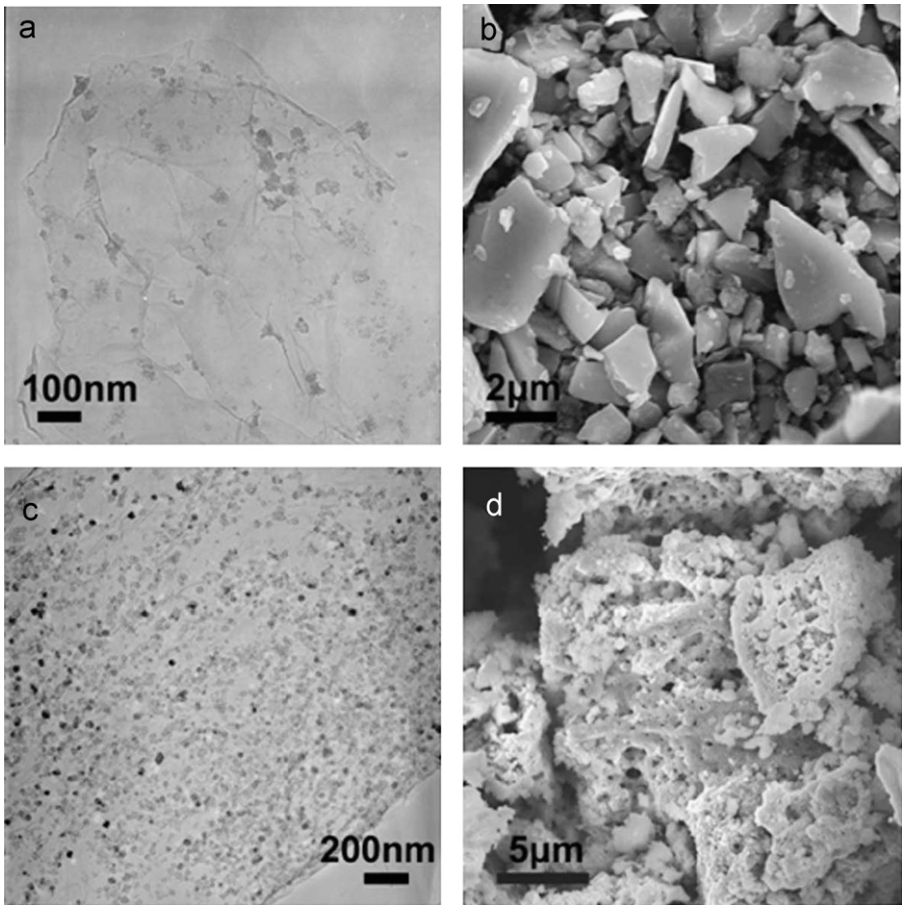

Figure 7 (a) TEM image of graphene/RuO_2 composite and (b) SEM image of RuO_2 without graphene under the same synthesis conditions [149]. (c) TEM image of graphene/Co_3O_4 composite and (d) SEM image of Co_3O_4 without graphene under the same synthesis conditions [117].

Author's personal copy

nanocrystalline TiO_2, rutile and anatase, with graphene for increased lithium ion insertion (Fig. 8) [137]. Moreover, this approach can be extended to produce other metal oxide nanostructures such as nanoneedles [151], nanowires [152], and semiconductor/metal catalysts [185] on 2D graphene.

The role of oxygen contained in graphene

A major advantage of graphene over other carbon materials such as graphite and CNTs is the presence of many oxygen-containing functional groups on the edges and surface of GO and reduced GO. These functional groups strongly influence the size, shape and distribution of metal oxide particles on the graphene. In order to clarify the effect of oxygen on the formation of metal oxide particles, we carried out comparative experiments on oxygen-rich and oxygen-free graphene for anchoring RuO_2 [149]. We used GO with a C/O ratio of <3 prepared by sonication and exfoliation of graphite oxide in aqueous solution, and CVD-grown graphene almost without any oxygen containing groups. Significantly, it was found that highly dispersed RuO_2 nanoparticles with a size less than 5 nm are formed on the surface of GO, while only large RuO_2 particles with a size ranging from tens to hundreds of nanometers are formed and sparsely distributed on the surface of CVD-grown graphene. This result strongly suggests that the presence of oxygen plays an important role in the formation and anchoring of well-dispersed fine nanoparticles on a 2D graphene support.

In another example, Dai and co-workers found that the size, morphology and crystallinity of nanocrystals are strongly dependant on the oxygen content of the underlying graphene substrate [186]. GNS with a low oxygen content of ~5% has weaker chemical interactions with coating species on the surface, resulting in the precoated small particles on GNS diffusing and recrystallizing into single crystal nanoplates with a well-defined shape due to fewer functional groups and defects (Fig. 9). In contrast, the highly oxidized GO (~20% of oxygen) surface with a high concentration of oxygen groups and defects interacts strongly with the precoated particles, offering a strong pinning force to the small particles that hinders diffusion and recrystallization and therefore results in irregular shaped nanocrystals. This work suggests that the size, morphology and crystallinity of nanoparticles can be tailored by the oxygen concentration of graphene substrates [186]. It is generally considered that metal oxides have interfacial interactions with GO [57,184] by both (i) reactive chemisorption on functional groups (such as HO-C=O and -OH) that bridge metal centers with carboxyl or hydroxyl groups at oxygen-defect sites and (ii) van der Waals interactions between the pristine region of graphene and metal oxides. Furthermore, by controlling the concentration of metal ions in solution and the amount of

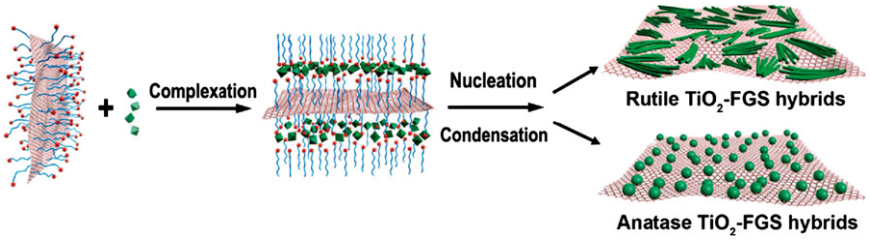

Figure 8 Anionic sulfate surfactant-mediated stabilization of graphene and growth of self-assembled TiO_2/few-layer graphene sheet (FGS) hybrid nanostructures. Reprinted with permission [137]. Copyright 2010, American Chemical Society.

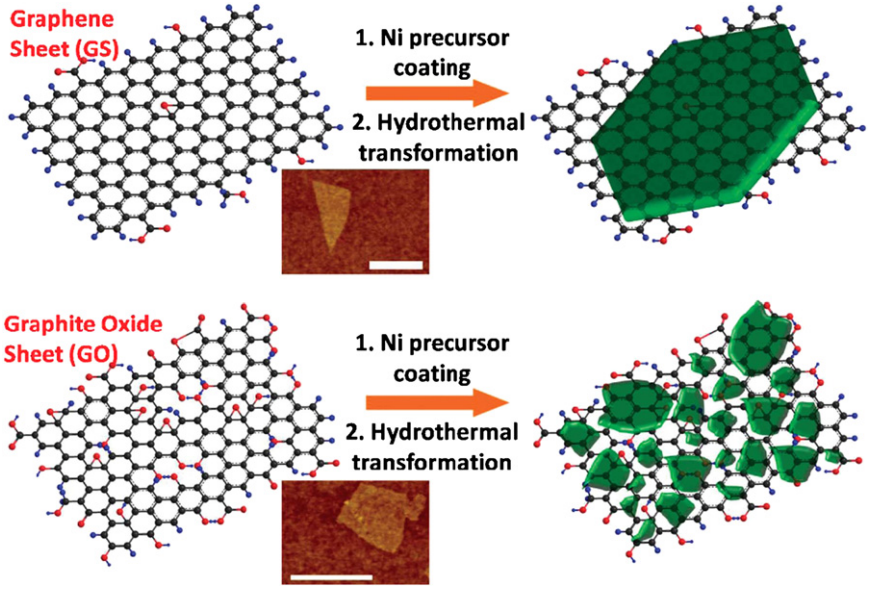

Figure 9 $Ni(OH)_2$ nanocrystal growth on a graphene sheet (GS, upper) and graphite oxide sheet (GO, lower) with 5% and 20% oxygen, respectively. Reprinted with permission [186]. Copyright 2010, American Chemical Society.

Author's personal copy

the graphene addition, it should also be possible to control the particle size of oxide nanoparticles. These findings may pave a way for the desired synthesis of novel graphene/metal oxide composites with controlled size, morphology and crystallinity using oxygen-defined graphene as a carbon support for LIBs and ECs.

Suppressing the re-stacking of graphene

Reduced graphene usually suffers from serious agglomeration and re-stacking after removal of suspension solvents due to the van der Waals interactions between adjacent sheets, therefore, leading to a great loss of effective surface area and consequently poorer electrochemical properties than expected. Therefore, keeping GNS from re-stacking plays a key role in improving the electrochemical performance of graphene-based materials in LIBs and ECs. Due to the synergistic effect between graphene and metal oxides, metal oxide nanoparticles supported on both side of graphene can serve as a nanospacer to separate the adjacent graphene sheets. The loading of metal oxide fine particles can inhibit or decrease the possibility of serious agglomeration and re-stacking of graphene and subsequently increase the available electrochemically-active surface area of graphene with a flexible porous structure for improving EDL capacitance. Wu et al. reported a sol–gel method to prepare hydrous RuO_2 nanoparticles anchored on graphene, in which nanosized RuO_2 serves as spacers to support GNS with an apparent increase in pore volume in this structure [149]. Yang et al. developed a bottom-up approach to prepare 2D sandwich-like graphene-based mesoporous silica (GM-silica), in which each graphene sheet is fully separated by a mesoporous silica cell [170]. The resulting GM-silica sheets are a perfect template for creating various 2D based nanosheets, such as mesoporous carbon, carbon nitride and metal oxide (Co_3O_4, TiO_2), with a sandwich-like structure [170–172]. For example, sandwich-like graphene–TiO_2 nanosheets exhibit a high rate capability and excellent cycle performance, having great potential as a high-rate anode material for lithium storage (Fig. 10) [172]. These results give clear evidence that fully separated graphene-based nanosheets not only increase the available surface area resulting in a higher electrochemical activity, but also significantly improve the electrochemical performance due to their favorable structures.

Constructing a 3D conductive network

Metal oxide-based electrodes generally suffer from poor electrical conductivity. To ensure a sufficient electrical conductivity of metal oxide electrodes during charge and discharge, conductive additives such as carbon black have to be added to optimize the electrical resistivity of the electrodes in electrode manufacturing but are not able to deliver energy in the charge–discharge process. Therefore, to maximize the energy density of an electrochemical cell, the amount of conductive carbon must be minimized, generally, below 10% of the total electrode mass. In addition to the amount of the additive, its texture and morphology also influence the conductivity of the electrodes. Different from the common conductive additives, graphene is not only a good electrically conductive carbon material but also an electrochemically active material. Therefore, graphene as a conductive carbon material in metal oxide electrodes is expected to construct a 3D conductive network among metal oxide particles [145,178].

Electrochemical impedance spectroscopy (EIS) is a powerful and accurate electrochemical technique for LIBs and ECs to examine the fundamental electrochemical behavior of electrodes, such as to determine the phenomenological electrode-solution interactions and discriminate between different contributions on the basis of their respective time constant. EIS analysis has been used to access the combined resistance of electrodes, electrolyte and current collectors in high frequency, charge transfer resistance with a semicircle in high-medium frequency, and the Warburg resistance in the lower frequency range that are interpreted with the help of equivalent circuit models. Depending on the fitting results of the EIS spectrum, Yang et al. showed that graphene-encapsulated Co_3O_4 (Fig. 11) composite has a significantly lower film resistance $R_f = 10.5\ \Omega$ and charge-transfer resistance $R_{ct} = 27.9\ \Omega$ than those of bare Co_3O_4 ($R_f = 27.8$ and $R_{ct} = 97.9\ \Omega$) [167]. Similar results with a lower interface impedence and a smaller depressed semicircle also were observed in the composites of graphene/$LiFePO_4$ [149] and graphene/$Li_4Ti_5O_{12}$ [178]. These results confirm that

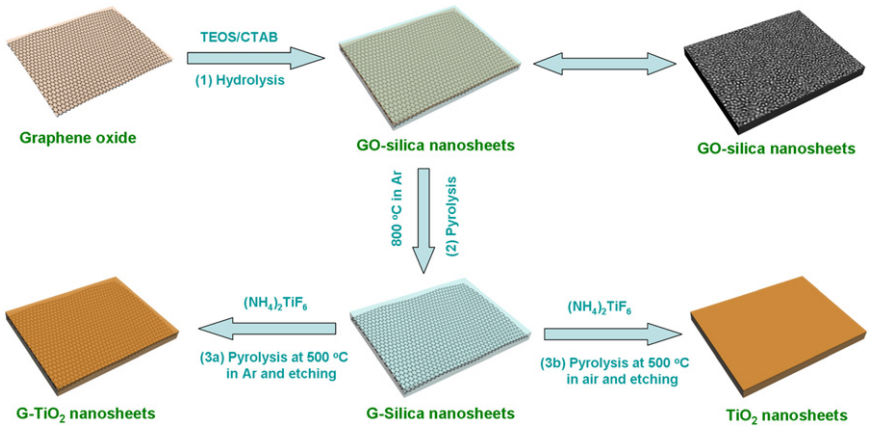

Figure 10 Fabrication of graphene-based titania (G-TiO_2) nanosheets and TiO_2 nanosheets without graphene. Reprinted with permission [172]. Copyright 2011, John Wiley & Sons, Inc.

Author's personal copy

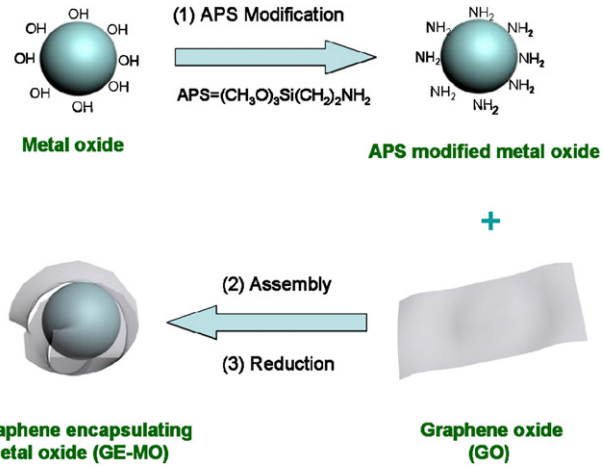

Figure 11 Fabrication schematic of a graphene-encapsulated metal oxide. Reprinted with permission [167]. Copyright 2010, John Wiley & Sons, Inc.

graphene can not only retain the high overall conductivity of the electrodes, but also greatly improve the electrochemical activity of metal oxides upon cycling.

Suppressing the volume change of metal oxides

Among a variety of electrode materials for LIBs, metal oxides such as SnO_2, Co_3O_4, and Fe_3O_4 with a high theoretical specific capacity have been considered as one of the most promising high-energy electrode candidates to substitute for current commercialized graphitic materials. However, these materials generally undergo severe structural and volume changes during lithium insertion and removal, leading to the pulverization of their electrodes and consequently fast capacity loss [187]. To use the high capacity feature of, and suppress the volume change of, metal oxide electrodes in a suitable manner, graphene with high electrical conductivity and mechanical flexibility is emerging as one of the most appealing matrices for improving the performance of metal oxides. Using this 2D ultrathin flexible structure, graphene-based 3D structures, such as metal oxide (Co_3O_4 [117], Mn_3O_4 [126], SnO_2 [103]) anchoring on graphene, graphene-wrapped metal oxide (Fe_3O_4 [162]) and graphene-encapsulated metal oxide (Co_3O_4 [167]) were reported, in which metal oxides are uniformly anchored onto the surface of graphene, or wrapped between graphene layers, or encapsulated by individual graphene sheets. Such graphene-based 3D structures exhibit a large elastic buffer space to accommodate the volume expansion/contraction of metal oxide particles and confine them during the Li insertion/extraction process. This efficiently prevents the aggregation and cracking or crumbling of the electrode material upon cycling, and thus retains the large capacity, good cycling performance and high rate capability. For example, Zhou et al. reported a 3D structure with graphene-wrapped Fe_3O_4 particles as an anode for high performance LIBs [162]. The morphology and microstructure of the commercial Fe_3O_4 particles and the graphene/Fe_3O_4 composite after 30 discharge/charge cycles were examined by SEM. It is observed that the commercial Fe_3O_4 particles are isolated and dispersed well in the initial state (Fig. 12a). However, after 30 cycles the particles become smaller and agglomerated (Fig. 12b), with the average size decreasing from 735 nm to 428 nm, indicating the pulverization of the particles during cycling. For the composite, the Fe_3O_4 particles are still closely embedded between graphene layers and the morphology and particle size are almost the same before (196 nm, Fig. 12c) and after (213 nm, Fig. 12d) cycling. It is suggested that the important role of graphene to flexibly wrap Fe_3O_4 particles can effectively accommodate the strain and stress of volume change during cycling.

Improving electrochemical properties of LIBs and ECs

The unique 2D structure of graphene offers multiple benefits in terms of constructing novel electrode materials. The following part highlights the improved electrochemical properties of metal oxide (such as SnO_2, Fe_3O_4, Co_3O_4, RuO_2, or MnO_2)/graphene composites as electrode materials in LIBs and ECs due to the synergistic effects. The electrochemical merits of graphene/metal oxide materials have been particularly addressed in comparison with their bulk oxide forms without the presence of graphene.

In order to understand the synergistic effects, Wu et al. investigated the experimental capacitance (C_{sp}^{exp}) of graphene/RuO_2 composites with different Ru loadings and their calculated capacitance (C_{sp}^{cal}) based on the pure GNS (C_{sp}^{GSs}, 148 F g^{-1}) and pure RuO_2 ($C_{sp}^{RuO_2}$, 606 F g^{-1}) based on the rule of mixture according to their weight ratios (Fig. 13) [149]. Importantly, it is found that the experimental capacitance C_{sp}^{exp} of the composites is much higher than the sum of the calculated capacitance (C_{sp}^{cal}) of the two simple individuals. The increased capacitance ($C_{sp}^{exp} - C_{sp}^{cal}$) strongly demonstrates the presence of synergistic effects between GNS and RuO_2 on improving the electrochemical performance of graphene/RuO_2 composites (Fig. 13). In fact, all improved electrochemical properties of graphene/metal oxide composites such as improved capacity/capacitance, cyclability, rate capability, and energy/power density can be attributed to these unique synergistic effects between metal oxide and graphene in an integrated 3D structure. Such synergistic effects are also observed in graphene/non-metal oxide composites for LIBs and ECs, such as GNS/polyaniline [188,189], graphene/$Co(OH)_2$ [190], graphene/$Ni(OH)_2$ [191], graphene/CNT [192], poly(sodium 4-styrensulfonate) intercalated GNS [193], Pt-exfoliated graphene [186], carbon black supported graphene[194], and graphene/Si [195].

Increased capacity/capacitance

A common electrochemical characteristic of graphene/metal oxide composites is to significantly increase the reversible capacity of LIBs or specific capacitance of ECs.

Tin-based oxides are considered as one of the most promising anode candidates to replace carbon-based materials due to their large theoretical capacity (i.e., 990 mA h g^{-1} for $Li_{4.4}Sn$) and good safety. Recently, Paek et al. reported a nanoporous 3D flexible graphene/SnO_2 composite with a delaminated structure by assembling SnO_2 nanoparticles on GNS in an ethylene glycol solution, which displays higher capacity and better

Author's personal copy

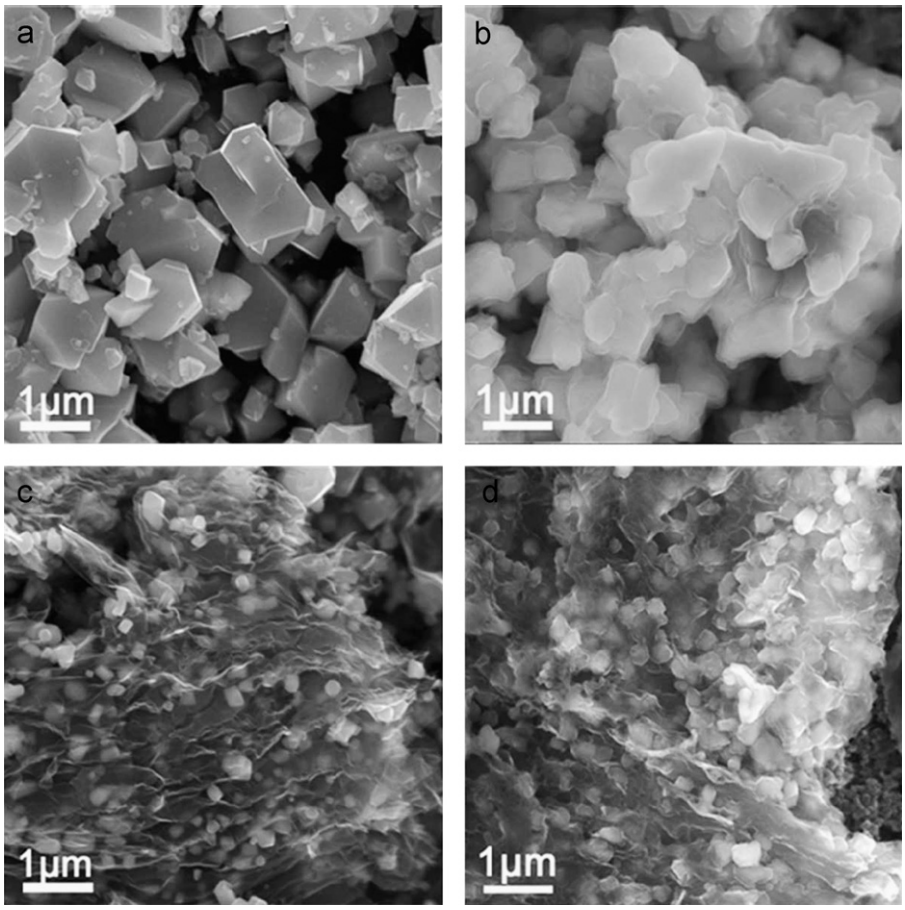

Figure 12 SEM images of (a, b) commercial Fe_3O_4 particles and (c, d) graphene/Fe_3O_4 composite before (a, c) and after (b, d) 30 discharge/charge cycles [162]. Copyright 2010, American Chemical Society.

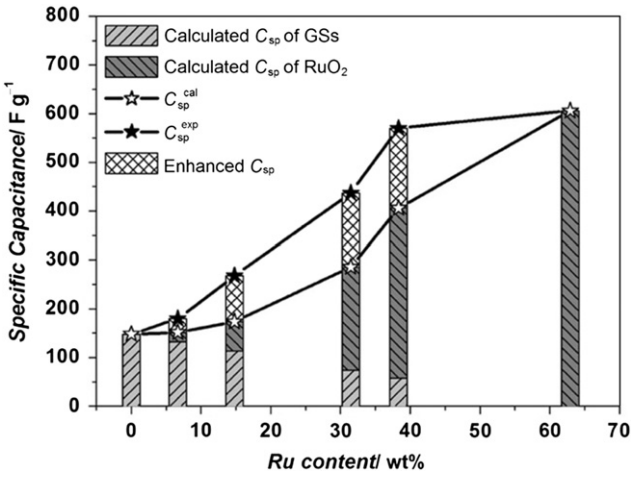

Figure 13 Experimental and calculated specific capacitance of graphene/RuO_2 composites (C_{sp}^{exp} and C_{sp}^{cal}). The calculated C_{sp}^{cal} of the composites is the sum of the calculated capacitance from GNS (GSs) and RuO_2 components based of the rule of mixture. The inter-cross slash line squares indicate the increased capacitance ($C_{sp}^{exp} - C_{sp}^{cal}$) due to the synergistic effects of GNS and RuO_2 in the composites. Reprinted with permission [149]. Copyright 2010, John Wiley & Sons, Inc.

cycling performance than that of SnO_2 without graphene (Fig. 14) [103]. The prepared GNS/SnO_2 exhibits an initial reversible capacity of 810 mA h g^{-1} and remains 570 mA h g^{-1} after 30 cycles, while the specific capacity of the bare SnO_2 nanoparticle on the first charge is 550 mA h g^{-1}, dropping rapidly to 60 mA h g^{-1} only after 15 cycles. Another example is that Kim et al. controlled surface charge to prepare echinoid-like SnO_2 nanoparticles uniformly decorated on GNS through electrostatic attraction between GNS and the echinoid-like SnO_2 particles. The GNS/SnO_2 composite shows much higher capacity and good cycling behavior compared to the commercial SnO_2. It retains a reversible capacity of 634 mA h g^{-1} with a coulombic efficiency of 98% after 50 cycles [107]. SnO_2 nanosheets hybrided with GNS have exhibited improved reversibility as well. Lou et al. developed a hydrothermal method to directly grow SnO_2 nanosheets on GNS. Electrochemical evaluations show that this unique GNS/SnO_2 hybrid structure exhibits greatly improved lithium storage properties compared to the pure SnO_2 nanosheets [113]. The superiority of the composites is ascribed to four factors: (1) the confinement of SnO_2 nanoparticles by surrounding GNS limits the volume expansion upon lithium insertion, (2) the pores developed between SnO_2 and GNS can be used as a buffer space during charge and discharge, (3) the 3D interconnected graphene framework suppresses nanoparticle aggregation, and (4) the

Author's personal copy

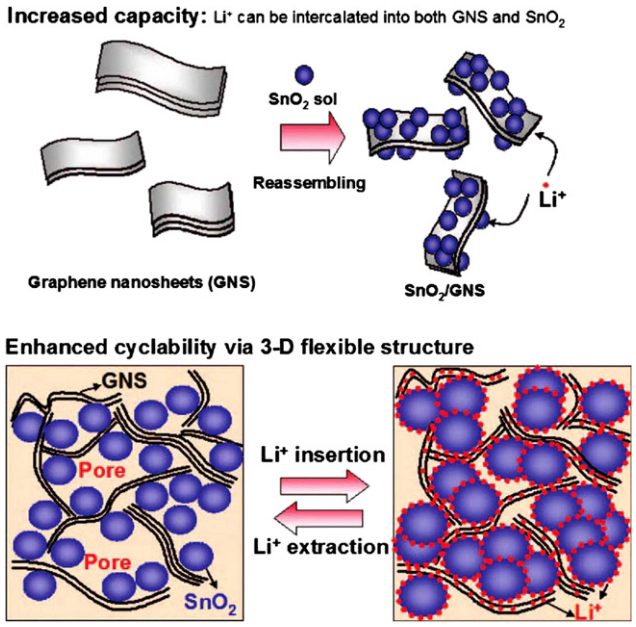

Figure 14 Schematic of the synthesis and structure of GNS/SnO_2. Reprinted with permission [103]. Copyright 2010, American Chemical Society.

electrically conducting graphene network ensures good electrical contacts. Another example of a 3D composite structure is to directly synthesize metal oxide nanoparticles anchored on graphene. Wu et al. reported a chemical *in-situ* deposition strategy to synthesize a composite of Co_3O_4 nanoparticles anchored on graphene as an anode material for high-performance LIBs [117]. It was found that the Co_3O_4 nanoparticles obtained are 10–30 nm in size and homogeneously anchored on the GNS which also functions as a spacer to keep the neighboring graphene sheets separated. This graphene/Co_3O_4 composite displays better electrochemical performance than Co_3O_4 and graphene. The first discharge and charge capacities are 2179 and 955 mA h g^{-1} for graphene, 1105 mA h g^{-1} and 817 mA h g^{-1} for Co_3O_4, and 1097 and ~753 mA h g^{-1} for the graphene/Co_3O_4 composite electrodes, respectively. But the reversible capacity of the composite electrode is as high as 900 mA h g^{-1} after 20 cycles, much better than that of Co_3O_4 (650 mA h g^{-1}) and graphene (245 mA h g^{-1}), highlighting the importance of anchoring nanoparticles on graphene for a better use of electrochemically active Co_3O_4 nanoparticles and graphene for high-performance LIBs. A similar attempt of fabricating graphene/Co_3O_4 hybrid material using *in situ* reduction process was reported by Kang's group. The hybrid is composed of 5 nm size Co_3O_4 particles uniformly dispersed on graphene, delivering a capacity of more than 800 mA h g^{-1} at a 200 mA g^{-1} rate and more than 550 mA h g^{-1} at a high current rate of 1000 mA g^{-1}. The superior electrochemical performance of the graphene/Co_3O_4 is due to its unique nanostructure, which intimately combines the conductive graphene network with uniformly dispersed Co_3O_4 nanoparticles [120]. Chen et al. reported the microwave-assisted synthesis of a Co_3O_4-graphene sheet-on-sheet nanostructure. The sheet-on-sheet composite shows a large capacity of 1235 mA h g^{-1} at 0.1 C and a capacity of 931 mA h g^{-1} is still obtained at a large rate of 5 C (4450 mA g^{-1}). The complementary synergetic effect of the composite is attributed to the prevented re-stacking of GNS, which are separated and stabilized by Co_3O_4 nanosheets, and increased electrical conductivity and mechanical stability of Co_3O_4 nanosheets in the presence of GNS [118]. It should be noted that the electrical conductivity of graphene plays a key role in improving the capacity of the electrodes, particularly for high rate anode materials such as $Li_4Ti_5O_{12}$ [178], TiO_2 [137], and cathode materials such as $LiFePO_4$ [145]. Ding et al. prepared nano-structured graphene/$LiFePO_4$ composites by co-precipitation, in which graphene is used as an additive to improve the electrical conductivity. It was found that the graphene/$LiFePO_4$ composites with only 1.5 wt% graphene deliver a higher specific capacity of 160 mA h g^{-1} than $LiFePO_4$ (113 mA h g^{-1}) as well as increasing its charge–discharge efficiency [145]. The above design concept is also extended to synthesize composite electrodes for high-performance ECs. For example, Fan et al. prepared GNS/Co_3O_4 composite by a microwave-assisted method. The well-dispersed Co_3O_4 nanoparticles (3–5 nm) on GNS greatly improve the electrochemical utilization of Co_3O_4 and double-layer capacitance from the interconnected open channels between graphene layers. The GNS/Co_3O_4 composite exhibits high specific capacitance (243.2 F g^{-1} at 10 mV s^{-1}) and excellent long cycle life (95.6% specific capacitance retained after 2000 cycles). The good results can be ascribed to that the GNS not only efficiently buffer the volume change of cobalt oxide during charge and discharge processes, but also preserve the high electrical conductivity of the overall electrode [148]. Another good example, benefitting from the combined advantages of graphene and RuO_2 in a anchored particle-sheet structure, graphene/RuO_2 composite-based ECs exhibit higher specific capacitance (~570 F g^{-1}) than that of graphene (148 F g^{-1}), which is due to the use of both graphene-based double layer capacitance and RuO_2-based pseudocapacitance [149]. The above results really demonstrate that synergistic effects between graphene and metal oxides play a critical role in improving the capacity/capacitance of the composites.

Improved cyclic performance

It is generally accepted that the Li-storage mechanism of metal oxides is based on either a lithium ion intercalation reaction or a lithium conversion reaction. The major drawback of metal oxide materials is that their capacity fades rapidly upon cycling, which is caused by a large volume change and/or by lower electrical conductivity. Therefore, many studies have been focused on the improvement of the cycling performance of metal oxides by suppressing their volume change and increasing their electrical conductivity. Graphene with intrinsically excellent electrical conductivity and mechanical flexibility is demonstrated as one of the most appealing carbon matrices for this purpose.

Among the graphene-based composites, metal oxide (SnO_2, Co_3O_4, Mn_3O_4, Cu_2O, etc.), nanoparticles anchored on graphene is most common for improving cyclability owning to the synergistic effect between graphene and metal oxides. For example, Wu et al. reported that the composite of Co_3O_4 nanoparticles anchored on graphene exhibits a much better cycling performance than graphene and Co_3O_4 [117]. The reversible capacity of graphene and Co_3O_4 decreases from 955 to 638 mA h g^{-1} and from 817 to 184 mA h g^{-1}, respectively, up to 30 cycles. In contrast, the

Author's personal copy

reversible capacity of the graphene/Co_3O_4 composite slightly increases with cycling, and reaches ~935 mA h g^{-1} after 30 cycles (Fig. 15a). Similarly, anchoring metal oxides on graphene was also reported to improve the cycling performance of ECs. Wu et al. reported that anchoring hydrous RuO_2 on graphene retains 97.9% of the original capacity after 1000 cycles, which is much better than that of a pure RuO_2 electrode (~42.0%) and graphene (90.9%) [149]. The excellent electrochemical stability is attributed to the 2D carbon support and double layer capacitance of graphene. Another important graphene-based structure is graphene-wrapped metal oxides, in which metal oxide particles are wrapped between adjacent graphene layers. For example, Zhou et al. reported that graphene-wrapped Fe_3O_4 composite shows a high reversible specific capacity of 1026 mA h g^{-1} after 30 cycles, which is much higher than that of commercial Fe_3O_4 (475 mA h g^{-1}) and bare Fe_2O_3 (359 mA h g^{-1}) with a rapid capacity fading (Fig. 15c) [162]. Recently, to effectively suppress the aggregation and accommodate the volume change of oxide nanoparticles upon cycling, Yang et al. developed a strategy to fabricate flexible, graphene-encapsulated metal oxides by electrostatic co-assembly between negatively charged GO and positively charged oxide nanoparticles, followed by chemical reduction [167]. The resulting graphene-encapsulated Co_3O_4 nanoparticles exhibit a high reversible capacity of 1100 mA h g^{-1} in the initial cycle, and over 1000 mA h g^{-1} after 130 cycles. Such graphene-based 3D structures have a large elastic buffer space to accommodate the volume change and prevent the aggregation of metal oxide particles during Li insertion/extraction, and efficiently suppress the cracking or crumbling of the electrode materials during cycling.

The above-mentioned examples suggest that designing 3D graphene-based structures with an elastic flexible framework are beneficial to their electrochemical performance in LIBs and ECs. Graphene as a 2D flexible support facilitates the formation of metal oxides with small sizes which strongly bind with graphene to suppress their volume change, improves the electrical conductivity of metal oxides and electrolyte contact, and shortens the transport distance of lithium ions and electrons, all of which are beneficial for improving the cycling performance of metal oxides.

Improved rate capability

Achieving high-rate capability for LIBs and ECs is also highly needed to meet the requirements in applications such as hybrid electric vehicles, electric vehicles and portable power tools at fast charge and discharge rates [196]. Nanostructured materials are expected to have a higher reversible accommodation of lithium at high rates than bulk

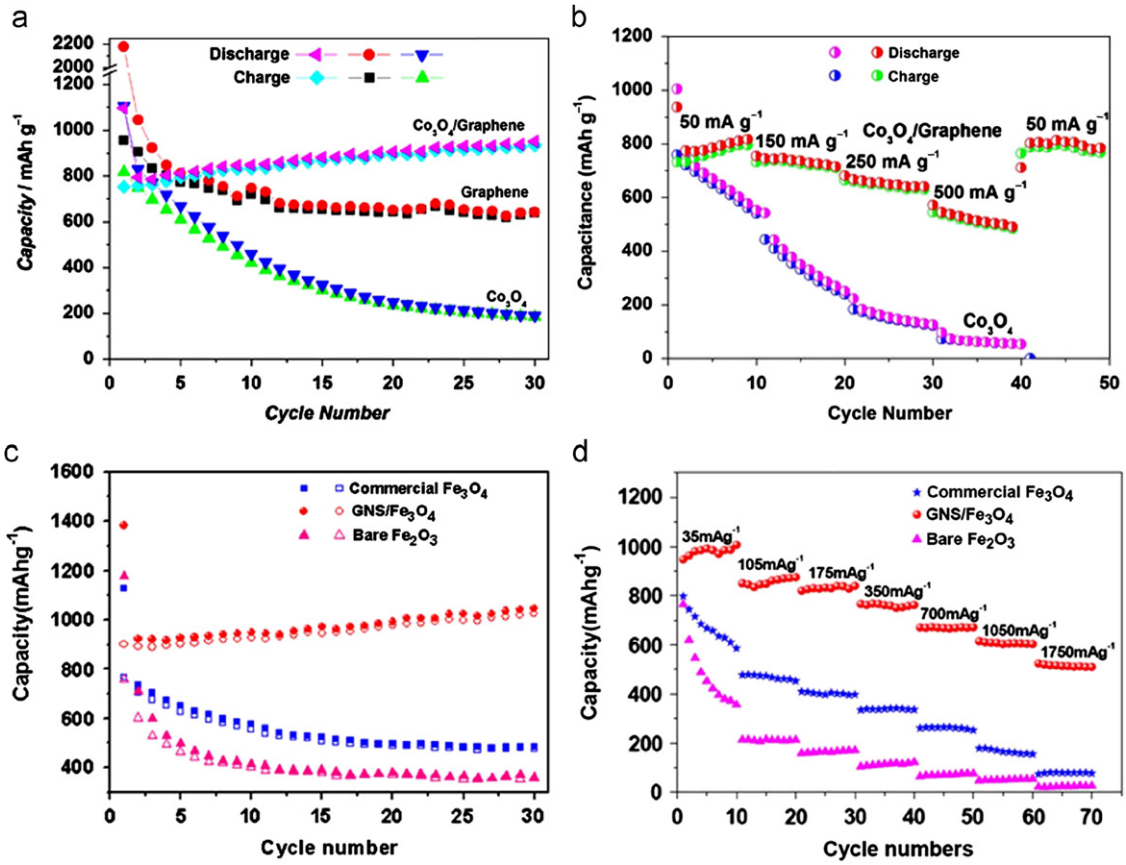

Figure 15 (a) Cycling performance of graphene, Co_3O_4 and graphene/Co_3O_4 composite. (b) Rate capability of graphene/Co_3O_4 composite and Co_3O_4 at various current densities. Reprinted with permission [117]. Copyright 2010, American Chemical Society. (c) Cycling performance and (d) rate performance of GNS/Fe_3O_4 composite, commercial Fe_3O_4 and bare Fe_2O_3. Reprinted with permission [162]. Copyright 2010, American Chemical Society.

Author's personal copy

materials due to the shortened distance of lithium ion and electron transport. However, the huge volume change and poor electrical conductivity of metal oxides during Li^+ insertion/extraction cycles inevitably result in rapid cracking and crumbling of the electrode, leading to the fast capacity loss of metal oxides (such as SnO_2 [103–108], Co_3O_4 [117–120,167], Fe_3O_4 [128,162]) based on the lithium conversion reaction and discontinuity of the electron path of metal oxides ($Li_4Ti_5O_{12}$ [178], TiO_2 [137], $LiFePO_4$ [138,145,149]) based on the lithium intercalation mechanism at high charge and discharge rates.

In the case of oxides for lithium conversion, it has been demonstrated that graphene-based composites exhibit a much better rate capability compared to bulk oxide electrodes by inhibiting the large volume change and providing good electron conduction paths [103,106–108, 117–120,137]. For example, Wu et al. reported that a graphene/Co_3O_4 composite retains a reversible capacity of 800 mA h g^{-1} at 50 mA g^{-1}, whereas the capacity of a Co_3O_4 electrode counterpart rapidly drops to 541 mA h g^{-1}. The reversible capacity of the Co_3O_4/graphene composite and Co_3O_4 at other rates is: 715 and 239 mA h g^{-1} at 150 mA g^{-1}, 631 and 122 mA h g^{-1} at 250 mA g^{-1}, and 484 and 53 mA h g^{-1} at 500 mA g^{-1}, respectively (Fig. 15b) [117]. The GNS/Fe_3O_4 composite exhibits a much better rate performance than commercial Fe_3O_4 and bare Fe_2O_3 particles. In particular, when the rate reaches a value as high as 1750 mA g^{-1}, the capacity of the composite is still 520 mA h g^{-1}, 53% of the initial capacity, while the capacities of Fe_3O_4 and Fe_2O_3 electrodes drop dramatically to 10% and 3% of the initial capacity at such a high rate (Fig. 15d) [162]. Similar results to improve rate capability were also reported for graphene/Mn_3O_4 [126], and graphene/SnO_2 [107,108].

A similar phenomenon is observed in graphene/metal oxide electrodes for ECs. Wu et al. reported that the specific capacitance of a graphene/RuO_2 composite electrode is much larger than that of a graphene electrode at the same scan rate [149]. Compared to pure RuO_2, the graphene/RuO_2 composite electrode not only exhibits a higher specific capacitance at high rates between 20 and 50 mV s^{-1}, but also presents a better rate capability of 47% than that of pure RuO_2 (36%). These results imply that graphene in graphene/RuO_2 composites is responsible for the improvement of high rate capability.

Larger energy/power density

Energy density (specific energy) is the amount of electrical energy stored in an energy storage cell, per unit of weight or volume, which are expressed as "gravimetric energy density" and "volumetric energy density" in terms of Watt-hour per unit mass (such as Wh kg^{-1}) or Watt-hour per unit volume (Wh L^{-1}), respectively. Power density (specific power) is defined as the ratio of available power from an energy storage cell to its weight or volume, which is typically expressed as gravimetric power density (usually W kg^{-1}) and volumetric power density (usually W L^{-1}). Both energy density and power density are the most important evaluation indices for a cell of LIBs or ECs, from which one can directly judge whether the cell reaches the practical goals or not, and both of them are generally expressed in a Ragone plot with power density vs. energy density.

It is well known that, in general, carbon electrodes with a high surface area have a higher power density while metal oxides with a large capacity/capacitance indicate the high energy density of an electrochemical cell. Therefore, graphene/metal oxide composites with a unique 3D structure are considered as high-energy and high-power electrode materials, including high energy LIBs based on high-capacity metal oxides (such as SnO_2 [103–108], Co_3O_4 [117–120,167], Fe_3O_4 [128,162]), high power LIBs based on high-rate metal oxides (such as TiO_2 [137]), and high energy and high power symmetric and asymmetric ECs (such as RuO_2 [149] and MnO_2 [78,151,152]), due to the possible maximum utilization and the combined effect of metal oxides and graphene. For example, Wu et al. reported that graphene/RuO_2 hybrid ECs display a high energy of 20.1 Wh kg^{-1} at a low power density (50 W kg^{-1}) although this value is slightly less than that of RuO_2 (22.2 Wh kg^{-1}), but much higher than that of GNS (3.1 Wh kg^{-1}), as shown in Fig. 16a. But the energy density of RuO_2 decreases rapidly to 1.3 Wh kg^{-1} (at 5000 W kg^{-1}) when the power density is more than 1000 W kg^{-1}. In sharp contrast, the graphene/RuO_2 composite still retains a high energy density of 7.2 Wh kg^{-1} at 5000 W kg^{-1} and 4.3 Wh kg^{-1} at a power density as high as

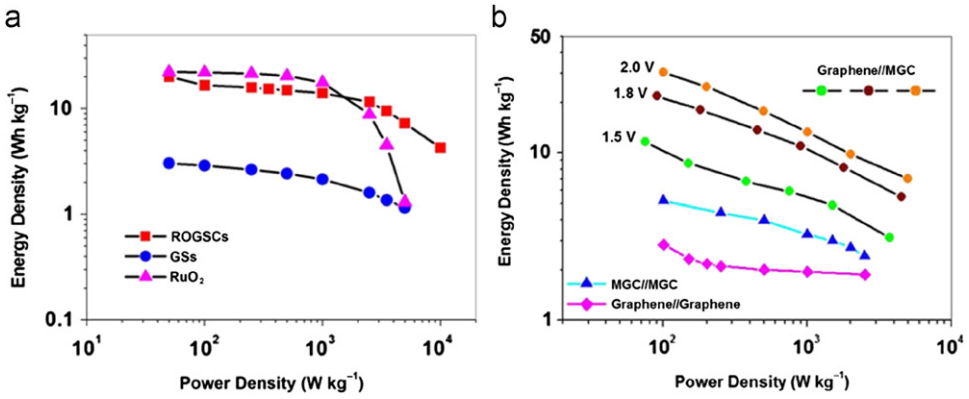

Figure 16 (a) Ragone plot for the as-prepared GNS, RuO_2 and graphene/RuO_2 composite (ROGSCs) ECs. Reprinted with permission [149]. Copyright 2010, John Wiley & Sons, Inc. (b) Ragone plot related to energy and power densities of graphene//MGC asymmetric ECs with various voltage windows, graphene//graphene and MGC//MGC symmetric ECs. Reprinted with permission [152]. Copyright 2010, American Chemical Society.

Author's personal copy

10000 W kg^{-1}. This good power characteristic of ECs takes full advantage of the graphene-based double layer capacitance and RuO_2 pseudocapacitance of graphene/RuO_2 composites, facilitating ion transport and increasing energy storage during the charge storage/delivery processes [149].

There is much interest in developing graphene-based asymmetric (hybrid) systems by combining a battery-like Faradic electrode (as energy source) and a capacitive carbon electrode (as power source) because this novel electrochemical device simultaneously offers the high power delivery of ECs (normally $\geq$1000 W kg^{-1}) and the high energy of LIBs (normally $\geq$10 Wh kg^{-1}), with a notable improvement of the energy density of high-power ECs. Very recently, Wu et al. developed high-voltage and high-energy asymmetric ECs based on a MnO_2 nanowire/graphene composite (MGC) as the positive electrode and graphene as the negative electrode in aqueous Na_2SO_4 solution [152]. This asymmetric EC exhibits a superior energy density of 30.4 Wh kg^{-1}, much higher than those of symmetrical ECs based on graphene//graphene (2.8 Wh kg^{-1}) and MGC//MGC (5.2 Wh kg^{-1}), and significantly higher than those of other aqueous MnO_2-based asymmetric ECs (Fig. 16b) [152]. It is noted that graphene and graphene-based composites open up good opportunities to develop high-energy hybrid electrochemical cells by reasonable material design and device construction.

Perspectives and challenges

We have reviewed the recent advance in electrochemical applications of graphene/metal oxide composite materials, highlighting them as a new and promising class of advanced electrode materials for LIBs and ECs. In these graphene-based materials, emphasis is given to synergistic effects between graphene and metal oxides. The beneficial role of graphene in the composites is due to its unique structures and properties such as high surface area, ultra-thin thickness, excellent electrical and thermal conductivity, mechanical flexibility, and high chemical functionality. Therefore, graphene can serve as an ideal 2D support for growing or assembling very small nanoparticles with well-defined structures, creating various graphene-based materials with excellent properties.

The synergistic effects in graphene/metal oxide composites can be briefly highlighted as follows: (i) graphene is a novel 2D support for uniformly nucleating, growing or assembling metal oxides with well-defined size, shape, and crystallinity; (ii) metal oxides between the layers of graphene can efficiently suppress the re-stacking of graphene; (iii) graphene can act as a 2D conductive template for building a 3D interconnected conductive porous network to improve the electrical conductivity and charge transport of pure oxides; (4) graphene can suppress the volume change and particle agglomeration of metal oxides during the charge–discharge process; (5) oxygen-containing functional groups on graphene ensures good interfacial interactions and electrical contacts between graphene and metal oxides. Due to these synergistic effects, integration of metal oxides and graphene in a composite fully uses each active component and consequently achieves excellent electrochemical performance in LIBs and ECs through materials design and fabrication.

Despite the short period of research, graphene/metal oxide composites with anchored, wrapped, encapsulated, layered, sandwich, mixed structures, etc., have confirmed the greatly improved electrochemical performance as electrodes of LIBs and ECs, such as increased capacity/capacitance, improved rate capability, improved cycling stability, and increased energy and power densities. It is noted that, among the various applications of graphene described in this review, LIBs and ECs have so far attracted more and more attention and are very likely to be commercially feasible in the near future through further optimization toward designing the graphene/metal oxide materials. However, several important challenges still urgently need to be overcome: (1) the controllability of the interface between graphene and metal oxides, especially, for EC and LIB applications that involve charge transfer processes. Unfortunately, most graphene/metal oxide materials reported so far are synthesized simply by mixing or dispersing their inorganic components with graphene, which leads to a poor interfacial interaction. A good understanding of surface chemistry on graphene and metal oxides is crucial for increasing interfacial interactions and thus achieving a well-defined uniform structure on graphene, especially, by modifying the surface chemistry using covalent or noncovalent techniques to increase the charge transfer. (2) Rational design and control of the morphology and phase composition of metal oxides on graphene can ensure reproducibility and better understanding of the structure–property relationships. Especially important is the fact that design and control of the texture and composition of the composites will possibly extend the potential use of graphene in many other applications. Given that chemically prepared graphene can be easily dispersed in solutions, a wide range of intriguing graphene-based composite electrodes can be created by *in situ* growth, covalent grafting or self-assembly. (3) Increasing interest should be directed to develop small, thin, lightweight and even flexible energy storage devices for advanced thin and wearable electronics. In this respect, graphene with unique properties of being ultrathin, lightweight (offering much higher power and energy with less device mass) and flexibile (working well even under twisting and bending conditions) will open up enormous opportunities for the fabrication of thin and flexible electrodes for thinner, smaller but high-power and high-energy ECs and LIBs. (4) New approaches to fabricate graphene-based composites have to involve a combined focus on new chemistry, controlled synthesis and device-performance of novel composite materials with optimized properties and functionalities, which is essential to improve the electrochemical performance of metal oxide/graphene composite materials for ECs and LIBs, and to creat novel graphene-based energy storage devices such as lithium air batteries, fuel cells, and organic electronics. (5) Considering the final industrial implementation, the successful application of graphene/metal oxide composites requires a comprehensive improvement in methodology and performance and better compatibility of the composites for use in the whole EC or LIB device, not merely high performance of the composite electrodes in some aspects. (6) The large-scale, low-cost and simple production of

Author's personal copy

graphene is among one of the most important challenges. (7) Understanding and clarifying the effects of the 2D structure of graphene and other 2D inorganic nanosheets on the electrochemical properties, such as lithium storage mechanism, relationship between lithium storage and defects, layer number, sizes and surface chemistry are also important. Future efforts should be focused on the control of the size, morphology, quantity and distribution of functional components and improving the interfacial interactions between graphene and functional building blocks. With continuous exploitation, it is believed that graphene/metal oxide composite materials for both LIBs and ECs will realize many practical applications such as in portable tools, personal electronics, electric vehicles, hybrid electric vehicles, and plug-in hybrid electric vehicles, etc.

Acknowledgment

This work was supported by the Key Research Program of Ministry of Science and Technology, China (no. 2011CB932604), the National Natural Science Foundation of China (no. 50921004), Chinese Academy Sciences (KGCX2-YW-231) and the Jinlu Limited.

References

[1] K.S. Novoselov, A.K. Geim, S.V. Morozov, D. Jiang, Y. Zhang, S.V. Dubonos, I.V. Grigorieva, A.A. Firsov, Science 306 (2004) 666–669.
[2] K.S. Novoselov, A.K. Geim, S.V. Morozov, D. Jiang, M.I. Katsnelson, I.V. Grigorieva, S.V. Dubonos, A.A. Firsov, Nature 438 (2005) 197–200.
[3] A.K. Geim, K.S. Novoselov, Nature Materials 6 (2007) 183–191.
[4] A.K. Geim, Science 324 (2009) 1530–1534.
[5] D.R. Dreyer, R.S. Ruoff, C.W. Bielawski, Angewandte Chemie International Edition 49 (2010) 9336–9344.
[6] K.S. Novoselov, D. Jiang, F. Schedin, T.J. Booth, V.V. Khotkevich, S.V. Morozov, A.K. Geim, Proceedings of the National Academy of Sciences of the United States of America 102 (2005) 10451–10453.
[7] V.I. Fal'ko, A.K. Geim, The European Physical Journal—Special Topics 148 (2007) 1–3.
[8] Y.B. Zhang, Y.W. Tan, H.L. Stormer, P. Kim, Nature 438 (2005) 201–204.
[9] Y. Kopelevich, P. Esquinazi, Advanced Materials 19 (2007) 4559–4563.
[10] S. Pisana, M. Lazzeri, C. Casiraghi, K.S. Novoselov, A.K. Geim, A.C. Ferrari, F. Mauri, Nature Materials 6 (2007) 198–201.
[11] F. Schedin, A.K. Geim, S.V. Morozov, E.W. Hill, P. Blake, M.I. Katsnelson, K.S. Novoselov, Nature Materials 6 (2007) 652–655.
[12] R.R. Nair, P. Blake, A.N. Grigorenko, K.S. Novoselov, T.J. Booth, T. Stauber, N.M.R. Peres, A.K. Geim, Science 320 (2008) 1308–1308.
[13] C.N.R. Rao, A.K. Sood, K.S. Subrahmanyam, A. Govindaraj, Angewandte Chemie International Edition 48 (2009) 7752–7777.
[14] C. Berger, Z.M. Song, T.B. Li, X.B. Li, A.Y. Ogbazghi, R. Feng, Z.T. Dai, A.N. Marchenkov, E.H. Conrad, P.N. First, W.A. de Heer, The Journal of Physical Chemistry B 108 (2004) 19912–19916.
[15] C. Berger, Z.M. Song, X.B. Li, X.S. Wu, N. Brown, C. Naud, D. Mayo, T.B. Li, J. Hass, A.N. Marchenkov, E.H. Conrad, P.N. First, W.A. de Heer, Science 312 (2006) 1191–1196.
[16] P.W. Sutter, J.I. Flege, E.A. Sutter, Nature Materials 7 (2008) 406–411.
[17] X.S. Li, W.W. Cai, J.H. An, S. Kim, J. Nah, D.X. Yang, R. Piner, A. Velamakanni, I. Jung, E. Tutuc, S.K. Banerjee, L. Colombo, R.S. Ruoff, Science 324 (2009) 1312–1314.
[18] A. Reina, X.T. Jia, J. Ho, D. Nezich, H.B. Son, V. Bulovic, M.S. Dresselhaus, J. Kong, Nano Letters 9 (2009) 30–35.
[19] Z.P. Chen, W.C. Ren, L.B. Gao, B.L. Liu, S.F. Pei, H.M. Cheng, Nature Materials 10 (2011) 424–428.
[20] S. Park, R.S. Ruoff, Nature Nanotechnology 4 (2009) 217–224.
[21] K.P. Loh, Q.L. Bao, P.K. Ang, J.X. Yang, Journal of Materials Chemistry 20 (2010) 2277–2289.
[22] J.N. Coleman, Advanced Functional Materials 19 (2009) 3680–3695.
[23] Z.S. Wu, W.C. Ren, L.B. Gao, B.L. Liu, J.P. Zhao, H.M. Cheng, Nano Research 3 (2010) 16–22.
[24] L.J. Zhi, K. Müllen, Journal of Materials Chemistry 18 (2008) 1472–1484.
[25] X.Y. Yang, X. Dou, A. Rouhanipour, L.J. Zhi, H.J. Rader, K. Müllen, Journal of the American Chemical Society 130 (2008) 4216–4217.
[26] N. Liu, F. Luo, H.X. Wu, Y.H. Liu, C. Zhang, J. Chen, Advanced Functional Materials 18 (2008) 1518–1525.
[27] Z.Z. Sun, Z. Yan, J. Yao, E. Beitler, Y. Zhu, J.M. Tour, Nature 468 (2010) 549–552.
[28] Y.P. Wu, B. Wang, Y.F. Ma, Y. Huang, N. Li, F. Zhang, Y.S. Chen, Nano Research 3 (2010) 661–669.
[29] M. Choucair, P. Thordarson, J.A. Stride, Nature Nanotechnology 4 (2009) 30–33.
[30] D.H. Deng, X.L. Pan, H. Zhang, Q.A. Fu, D.L. Tan, X.H. Bao, Advanced Materials 22 (2010) 2168–2171.
[31] Y.W. Zhu, S. Murali, W.W. Cai, X.S. Li, J.W. Suk, J.R. Potts, R.S. Ruoff, Advanced Materials 22 (2010) 3906–3924.
[32] C. Soldano, A. Mahmood, E. Dujardin, Carbon 48 (2010) 2127–2150.
[33] W. Hummers, R. Offman, Journal of the American Chemical Society 80 (1958) 1339.
[34] S. Stankovich, D.A. Dikin, R.D. Piner, K.A. Kohlhaas, A. Kleinhammes, Y. Jia, Y. Wu, S.T. Nguyen, R.S. Ruoff, Carbon 45 (2007) 1558–1565.
[35] H.C. Schniepp, J.L. Li, M.J. McAllister, H. Sai, M. Herrera-Alonso, D.H. Adamson, R.K. Prud'homme, R. Car, D.A. Saville, I.A. Aksay, The Journal of Physical Chemistry B 110 (2006) 8535–8539.
[36] M.J. McAllister, J.L. LiO, D.H. Adamson, H.C. Schniepp, A.A. Abdala, J. Liu, M. Herrera-Alonso, D.L. Milius, R. CarO, R.K. Prud'homme, I.A. Aksay, Chemistry of Materials 19 (2007) 4396–4404.
[37] Z.S. Wu, W. Ren, L. Gao, B. Liu, C. Jiang, H.M. Cheng, Carbon 47 (2009) 493–499.
[38] Z.S. Wu, W. Ren, L. Gao, J. Zhao, Z. Chen, B. Liu, D. Tang, B. Yu, C. Jiang, H.M. Cheng, ACS Nano 3 (2009) 411–417.
[39] X.B. Fan, W.C. Peng, Y. Li, X.Y. Li, S.L. Wang, G.L. Zhang, F.B. Zhang, Advanced Materials 20 (2008) 4490–4493.
[40] H.J. Shin, K.K. Kim, A. Benayad, S.M. Yoon, H.K. Park, I.S. Jung, M.H. Jin, H.K. Jeong, J.M. Kim, J.Y. Choi, Y.H. Lee, Advanced Functional Materials 19 (2009) 1987–1992.
[41] S.F. Pei, J.H. Du, J.P. Zhao, W.C. Ren, H.M. Cheng, Carbon 48 (2010) 4466–4474.
[42] J.I. Paredes, S. Villar-Rodil, A. Martinez-Alonso, J.M.D. Tascon, Langmuir 24 (2008) 10560–10564.
[43] T. Ramanathan, A.A. Abdala, S. Stankovich, D.A. Dikin, M. Herrera-Alonso, R.D. Piner, D.H. Adamson, H.C. Schniepp, X. Chen, R.S. Ruoff, S.T. Nguyen, I.A. Aksay, R.K. Prud'homme, L.C. Brinson, Nature Nanotechnology 3 (2008) 327–331.
[44] G.C. Liang, N. Neophytou, M.S. Lundstrom, D.E. Nikonov, Journal of Applied Physics 102 (2007) 054307.

Author's personal copy

[45] O.V. Yazyev, M.I. Katsnelson, Physical Review Letters 100 (2008) 047209.
[46] I. Meric, M.Y. Han, A.F. Young, B. Ozyilmaz, P. Kim, K.L. Shepard, Nature Nanotechnology 3 (2008) 654–659.
[47] F. Bonaccorso, Z. Sun, T. Hasan, A.C. Ferrari, Nature Photonics 4 (2010) 611–622.
[48] D.A. Dikin, S. Stankovich, E.J. Zimney, R.D. Piner, G.H.B. Dommett, G. Evmenenko, S.T. Nguyen, R.S. Ruoff, Nature 448 (2007) 457–460.
[49] S. Stankovich, D.A. Dikin, G.H.B. Dommett, K.M. Kohlhaas, E.J. Zimney, E.A. Stach, R.D. Piner, S.T. Nguyen, R.S. Ruoff, Nature 442 (2006) 282–286.
[50] K.S. Kim, Y. Zhao, H. Jang, S.Y. Lee, J.M. Kim, K.S. Kim, J.H. Ahn, P. Kim, J.Y. Choi, B.H. Hong, Nature 457 (2009) 706–710.
[51] S. Bae, H. Kim, Y. Lee, X.F. Xu, J.S. Park, Y. Zheng, J. Balakrishnan, T. Lei, H.R. Kim, Y.I. Song, Y.J. Kim, K.S. Kim, B. Ozyilmaz, J.H. Ahn, B.H. Hong, S. Iijima, Nature Nanotechnology 5 (2010) 574–578.
[52] H. Chen, M.B. Muller, K.J. Gilmore, G.G. Wallace, D. Li, Advanced Materials 20 (2008) 3557–3561.
[53] M. Pumera, The Chemical Record 9 (2009) 211–223.
[54] X. Wang, L.J. Zhi, K. Müllen, Nano Letters 8 (2008) 323–327.
[55] X. Wang, L.J. Zhi, N. Tsao, Z. Tomovic, J.L. Li, K. Müllen, Angewandte Chemie International Edition 47 (2008) 2990–2992.
[56] Z.S. Wu, S. Pei, W. Ren, D. Tang, L. Gao, B. Liu, F. Li, C. Liu, H.M. Cheng, Advanced Materials 21 (2009) 1756–1760.
[57] I.V. Lightcap, T.H. Kosel, P.V. Kamat, Nano Letters 10 (2010) 577–583.
[58] G. Williams, B. Seger, P.V. Kamat, ACS Nano 2 (2008) 1487–1491.
[59] D. Choi, M.Y. Choi, W.M. Choi, H.J. Shin, H.K. Park, J.S. Seo, J. Park, S.M. Yoon, S.J. Chae, Y.H. Lee, S.W. Kim, J.Y. Choi, S.Y. Lee, J.M. Kim, Advanced Materials 22 (2010) 2187–2192.
[60] L.P. Ma, Z.S. Wu, J. Li, E.D. Wu, W. Ren, H.M. Cheng, International Journal of Hydrogen Energy 34 (2009) 2329–2332.
[61] M. Pumera, Chemical Society Reviews 39 (2010) 4146–4157.
[62] W. Choi, I. Lahiri, R. Seelaboyina, Y.S. Kang, Critical Reviews in Solid State and Materials Sciences 35 (2010) 52–71.
[63] D.C. Wei, Y.Q. Liu, Advanced Materials 22 (2010) 3225–3241.
[64] M. Winter, J.O. Besenhard, M.E. Spahr, P. Novak, Advanced Materials 10 (1998) 725–763.
[65] C. Masarapu, V. Subramanian, H.W. Zhu, B.Q. Wei, Advanced Functional Materials 19 (2009) 1008–1014.
[66] C. Kim, K.S. Yang, M. Kojima, K. Yoshida, Y.J. Kim, Y.A. Kim, M. Endo, Advanced Functional Materials 16 (2006) 2393–2397.
[67] H.Q. Li, R.L. Liu, D.Y. Zhao, Y.Y. Xia, Carbon 45 (2007) 2628–2635.
[68] Y.S. Hu, P. Adelhelm, B.M. Smarsly, S. Hore, M. Antonietti, J. Maier, Advanced Functional Materials 17 (2007) 1873–1878.
[69] A. Mabuchi, K. Tokumitsu, H. Fujimoto, T. Kasuh, Journal of The Electrochemical Society 142 (1995) 1041–1046.
[70] J.R. Dahn, T. Zheng, Y.H. Liu, J.S. Xue, Science 270 (1995) 590–593.
[71] K. Sato, M. Noguchi, A. Demachi, N. Oki, M. Endo, Science 264 (1994) 556–558.
[72] E. Yoo, J. Kim, E. Hosono, H. Zhou, T. Kudo, I. Honma, Nano Letters 8 (2008) 2277–2282.
[73] G.X. Wang, X.P. Shen, J. Yao, J. Park, Carbon 47 (2009) 2049–2053.
[74] P. Guo, H.H. Song, X.H. Chen, Electrochemistry Communications 11 (2009) 1320–1324.
[75] P.C. Lian, X.F. Zhu, S.Z. Liang, Z. Li, W.S. Yang, H.H. Wang, Electrochimica Acta 55 (2010) 3909–3914.
[76] D.Y. Pan, S. Wang, B. Zhao, M.H. Wu, H.J. Zhang, Y. Wang, Z. Jiao, Chemistry of Materials 21 (2009) 3136–3142.
[77] C.Y. Wang, D. Li, C.O. Too, G.G. Wallace, Chemistry of Materials 21 (2009) 2604–2606.
[78] Z.S. Wu, W.C. Ren, L. Xu, F. Li, H.M. Cheng, ACS Nano 5 (2011) 5463–5471.
[79] D.S. Su, R. Schlogl, ChemSusChem 3 (2010) 136–168.
[80] N.A. Kaskhedikar, J. Maier, Advanced Materials 21 (2009) 2664–2680.
[81] G.G. Wallace, J. Chen, D. Li, S.E. Moulton, J.M. Razal, Journal of Materials Chemistry 20 (2010) 3553–3562.
[82] H. Bai, C. Li, G.Q. Shi, Advanced Materials 23 (2011) 1089–1115.
[83] M.H. Liang, L.J. Zhi, Journal of Materials Chemistry 19 (2009) 5871–5878.
[84] P. Simon, Y. Gogotsi, Nature Materials 7 (2008) 845–854.
[85] C. Liu, F. Li, L.P. Ma, H.M. Cheng, Advanced Materials 22 (2010) 28–62.
[86] L.L. Zhang, R. Zhou, X.S. Zhao, Journal of Materials Chemistry 20 (2010) 5983–5992.
[87] S.R.C. Vivekchand, C.S. Rout, K.S. Subrahmanyam, A. Govindaraj, C.N.R. Rao, Journal of Chemical Sciences 120 (2008) 9–13.
[88] Y. Wang, Z.Q. Shi, Y. Huang, Y.F. Ma, C.Y. Wang, M.M. Chen, Y.S. Chen, The Journal of Physical Chemistry C 113 (2009) 13103–13107.
[89] W. Lv, D.M. Tang, Y.B. He, C.H. You, Z.Q. Shi, X.C. Chen, C.M. Chen, P.X. Hou, C. Liu, Q.H. Yang, ACS Nano 3 (2009) 3730–3736.
[90] M.D. Stoller, S.J. Park, Y.W. Zhu, J.H. An, R.S. Ruoff, Nano Letters 8 (2008) 3498–3502.
[91] Y.W. Zhu, S. Murali, M.D. Stoller, A. Velamakanni, R.D. Piner, R.S. Ruoff, Carbon 48 (2010) 2118–2122.
[92] Y.W. Zhu, M.D. Stoller, W.W. Cai, A. Velamakanni, R.D. Piner, D. Chen, R.S. Ruoff, ACS Nano 4 (2010) 1227–1233.
[93] D.W. Wang, F. Li, Z.S. Wu, W. Ren, H.M. Cheng, Electrochemistry Communications 11 (2009) 1729–1732.
[94] J.L. Xia, F. Chen, J.H. Li, N.J. Tao, Nature Nanotechnology 4 (2009) 505–509.
[95] C.G. Liu, Z.N. Yu, D. Neff, A. Zhamu, B.Z. Jang, Nano Letters 10 (2010) 4863–4868.
[96] J.R. Miller, R.A. Outlaw, B.C. Holloway, Science 329 (2010) 1637–1639.
[97] A.V. Murugan, T. Muraliganth, A. Manthiram, Chemistry of Materials 21 (2009) 5004–5006.
[98] J.M. Tarascon, M. Armand, Nature 414 (2001) 359–367.
[99] P. Poizot, S. Laruelle, S. Grugeon, L. Dupont, J.M. Tarascon, Nature 407 (2000) 496–499.
[100] C.M. Park, J.H. Kim, H. Kim, H.J. Sohn, Chemical Society Reviews 39 (2010) 3115–3141.
[101] J. Cabana, L. Monconduit, D. Larcher, M.R. Palacin, Advanced Materials 22 (2010) E170–E192.
[102] L.W. Ji, Z. Lin, M. Alcoutlabi, X.W. Zhang, Energy & Environmental Science 4 (2011) 2682–2699.
[103] S.M. Paek, E. Yoo, I. Honma, Nano Letters 9 (2009) 72–75.
[104] J. Yao, X.P. Shen, B. Wang, H.K. Liu, G.X. Wang, Electrochemistry Communications 11 (2009) 1849–1852.
[105] L.S. Zhang, L.Y. Jiang, H.J. Yan, W.D. Wang, W. Wang, W.G. Song, Y.G. Guo, L.J. Wan, Journal of Materials Chemistry 20 (2010) 5462–5467.
[106] Z.F. Du, X.M. Yin, M. Zhang, Q.Y. Hao, Y.G. Wang, T.H. Wang, Materials Letters 64 (2010) 2076–2079.
[107] H. Kim, S.W. Kim, Y.U. Park, H. Gwon, D.H. Seo, Y. Kim, K. Kang, Nano Research 3 (2010) 813–821.
[108] Z.Y. Wang, H. Zhang, N. Li, Z.J. Shi, Z.N. Gu, G.P. Cao, Nano Research 3 (2010) 748–756.
[109] M. Zhang, D. Lei, Z.F. Du, X.M. Yin, L.B. Chen, Q.H. Li, Y.G. Wang, T.H. Wang, Journal of Materials Chemistry 21 (2011) 1673–1676.
[110] X.D. Huang, X.F. Zhou, L.A. Zhou, K. Qian, Y.H. Wang, Z.P. Liu, C.Z. Yu, ChemPhysChem 12 (2011) 278–281.
[111] P. Lian, X. Zhu, S. Liang, Z. Li, W. Yang, H. Wang, Electrochimica Acta 56 (2011) 4532–4539.

Author's personal copy

[112] X. Wang, X. Zhou, K. Yao, J. Zhang, Z. Liu, Carbon 49 (2011) 133–139.
[113] S. Ding, D. Luan, F.Y.C. Boey, J.S. Chen, X.W. Lou, Chemical Communications 47 (2011) 7155–7157.
[114] X. Zhu, Y. Zhu, S. Murali, M.D. Stoller, R.S. Ruoff, Journal of Power Sources 196 (2011) 6473–6477.
[115] B. Zhao, G. Zhang, J. Song, Y. Jiang, H. Zhuang, P. Liu, T. Fang, Electrochimica Acta 56 (2011) 7340–7346.
[116] B. Zhang, Q.B. Zheng, Z.D. Huang, S.W. Oh, J.K. Kim, Carbon 49 (2011) 4524–4534.
[117] Z.S. Wu, W.C. Ren, L. Wen, L.B. Gao, J.P. Zhao, Z.P. Chen, G.M. Zhou, F. Li, H.M. Cheng, ACS Nano 4 (2010) 3187–3194.
[118] S.Q. Chen, Y. Wang, Journal of Materials Chemistry 20 (2010) 9735–9739.
[119] G. Wang, J. Liu, S. Tang, H. Li, Journal of Solid State Electrochemistry (2010) 10.1007/s10008-10010-11254-y.
[120] H. Kim, D.H. Seo, S.W. Kim, J. Kim, K. Kang, Carbon 49 (2011) 326–332.
[121] B.J. Li, H.Q. Cao, J. Shao, G.Q. Li, M.Z. Qu, G. Yin, Inorganic Chemistry 50 (2011) 1628–1632.
[122] J. Zhu, Y.K. Sharma, Z. Zeng, X. Zhang, M. Srinivasan, S. Mhaisalkar, H. Zhang, H.H. Hng, Q. Yan, The Journal of Physical Chemistry C 115 (2011) 8400–8406.
[123] B. Wang, Y. Wang, J. Park, H. Ahn, G. Wang, Journal of Alloys and Compounds 509 (2011) 7778–7783.
[124] X. Zhu, Y. Zhu, S. Murali, M.D. Stoller, R.S. Ruoff, ACS Nano 5 (2011) 3333–3338.
[125] W. Zhou, J. Zhu, C. Cheng, J. Liu, H. Yang, C. Cong, C. Guan, X. Jia, H.J. Fan, Q. Yan, C.M. Li, T. Yu, Energy & Environmental Science (2011) 10.1039/C1031EE02168K.
[126] H.L. Wang, L.F. Cui, Y.A. Yang, H.S. Casalongue, J.T. Robinson, Y.Y. Liang, Y. Cui, H.J. Dai, Journal of the American Chemical Society 132 (2010) 13978–13980.
[127] C.-T. Hsieh, C.-Y. Lin, J.-Y. Lin, Electrochimica Acta 56 (2011) 8861–8867.
[128] M. Zhang, D.N. Lei, X.M. Yin, L.B. Chen, Q.H. Li, Y.G. Wang, T.H. Wang, Journal of Materials Chemistry 20 (2010) 5538–5543.
[129] S.K. Behera, Chemical Communications 47 (2011) 10371–10373.
[130] J. Su, M. Cao, L. Ren, C. Hu, The Journal of Physical Chemistry C 115 (2011) 14469–14477.
[131] J. Zhou, H. Song, L. Ma, X. Chen, RSC Advances 1 (2011) 782–791.
[132] L. Ji, Z. Tan, T.R. Kuykendall, S. Aloni, S. Xun, E. Lin, V. Battaglia, Y. Zhang, Physical Chemistry Chemical Physics 13 (2011) 7170–7177.
[133] B. Li, H. Cao, J. Shao, M. Qu, J.H. Warner, Journal of Materials Chemistry 21 (2011) 5069–5075.
[134] B. Li, H. Cao, J. Shao, M. Qu, Chemical Communications 47 (2011) 10374–10376.
[135] I.R.M. Kottegoda, N.H. Idris, L. Lu, J.-Z. Wang, H.-K. Liu, Electrochimica Acta 56 (2011) 5815–5822.
[136] J. Hu, A. Ramadan, F. Luo, B. Qi, X. Deng, J. Chen, Journal of Materials Chemistry 21 (2011) 15009–15014.
[137] D.H. Wang, D.W. Choi, J. Li, Z.G. Yang, Z.M. Nie, R. Kou, D.H. Hu, C.M. Wang, L.V. Saraf, J.G. Zhang, I.A. Aksay, J. Liu, ACS Nano 3 (2009) 907–914.
[138] D.W. Choi, D.H. Wang, V.V. Viswanathan, I.T. Bae, W. Wang, Z.M. Nie, J.G. Zhang, G.L. Graff, J. Liu, Z.G. Yang, T. Duong, Electrochemistry Communications 12 (2010) 378–381.
[139] S. Ding, J.S. Chen, D. Luan, F.Y.C. Boey, S. Madhavi, X.W. Lou, Chemical Communications 47 (2011) 5780–5782.
[140] B. Wang, X.-L. Wu, C.-Y. Shu, Y.-G. Guo, C.-R. Wang, Journal of Materials Chemistry 20 (2010) 10661–10664.
[141] Y.J. Mai, X.L. Wang, J.Y. Xiang, Y.Q. Qiao, D. Zhang, C.D. Gu, J.P. Tu, Electrochimica Acta 56 (2011) 2306–2311.
[142] J. Zhou, L. Ma, H. Song, B. Wu, X. Chen, Electrochemistry Communications (2011) doi:10.1016/j.elecom.2011.1008.1011.
[143] C. Xu, X. Wang, L.C. Yang, Y.P. Wu, Journal of Solid State Chemistry 182 (2009) 2486–2490.
[144] B. Li, H. Cao, G. Yin, Y. Lu, J. Yin, Journal of Materials Chemistry 21 (2011) 10645–10648.
[145] Y. Ding, Y. Jiang, F. Xu, J. Yin, H. Ren, Q. Zhuo, Z. Long, P. Zhang, Electrochemistry Communications 12 (2010) 10–13.
[146] G. Wang, J. Bai, Y. Wang, Z. Ren, J. Bai, Scripta Materialia 65 (2011) 339–342.
[147] W. Zhou, J. Liu, T. Chen, K.S. Tan, X. Jia, Z. Luo, C. Cong, H. Yang, C.M. Li, T. Yu, Physical Chemistry Chemical Physics 13 (2011) 14462–14465.
[148] J. Yan, T. Wei, W.M. Qiao, B. Shao, Q.K. Zhao, L.J. Zhang, Z.J. Fan, Electrochimica Acta 55 (2010) 6973–6978.
[149] Z.S. Wu, D.W. Wang, W. Ren, J. Zhao, G. Zhou, F. Li, H.M. Cheng, Advanced Functional Materials 20 (2010) 3595–3602.
[150] A.K. Mishra, S. Ramaprabhu, The Journal of Physical Chemistry C 115 (2011) 14006–14013.
[151] S. Chen, J.W. Zhu, X.D. Wu, Q.F. Han, X. Wang, ACS Nano 4 (2010) 2822–2830.
[152] Z.S. Wu, W.C. Ren, D.W. Wang, F. Li, B.L. Liu, H.M. Cheng, ACS Nano 4 (2010) 5835–5842.
[153] J. Zhang, J. Jiang, X.S. Zhao, The Journal of Physical Chemistry C 115 (2011) 6448–6454.
[154] Y. Qian, S. Lu, F. Gao, Journal of Materials Science 46 (2011) 3517–3522.
[155] Q. Cheng, J. Tang, J. Ma, H. Zhang, N. Shinya, L.-C. Qin, Carbon 49 (2011) 2917–2925.
[156] H. Huang, X. Wang, Nanoscale 3 (2011) 3185–3191.
[157] G. Yu, L. Hu, M. Vosgueritchian, H. Wang, X. Xie, J.R. McDonough, X. Cui, Y. Cui, Z. Bao, Nano Letters 11 (2011) 2905–2911.
[158] Z. Fan, J. Yan, T. Wei, L. Zhi, G. Ning, T. Li, F. Wei, Advanced Functional Materials 21 (2011) 2366–2375.
[159] B. Wang, J. Park, C.Y. Wang, H. Ahn, G.X. Wang, Electrochimica Acta 55 (2010) 6812–6817.
[160] Y.P. Zhang, H.B. Li, L.K. Pan, T. Lu, Z. Sun, Journal of Electroanalytical Chemistry 634 (2009) 68–71.
[161] J. Wang, Z. Gao, Z. Li, B. Wang, Y. Yan, Q. Liu, T. Mann, M. Zhang, Z. Jiang, Journal of Solid State Chemistry 184 (2011) 1421–1427.
[162] G.M. Zhou, D.W. Wang, F. Li, L.L. Zhang, N. Li, Z.S. Wu, L. Wen, G.Q. Lu, H.M. Cheng, Chemistry of Materials 22 (2010) 5306–5313.
[163] J.S. Chen, Z. Wang, X.C. Dong, P. Chen, X.W. Lou, Nanoscale 3 (2011) 2158–2161.
[164] W. Lv, F. Sun, D.-M. Tang, H.-T. Fang, C. Liu, Q.-H. Yang, H.-M. Cheng, Journal of Materials Chemistry 21 (2011) 9014–9019.
[165] Y. Sun, X. Hu, W. Luo, Y. Huang, ACS Nano 5 (2011) 7100–7107.
[166] H. Liu, W. Yang, Energy & Environmental Science 4 (2011) 4000–4008.
[167] S.B. Yang, X.L. Feng, S. Ivanovici, K. Müllen, Angewandte Chemie International Edition 49 (2010) 8408–8411.
[168] J.Z. Wang, C. Zhong, D. Wexler, N.H. Idris, Z.X. Wang, L.Q. Chen, H.K. Liu, Chemistry—A European Journal 17 (2011) 661–667.
[169] D. Chen, G. Ji, Y. Ma, J.Y. Lee, J. Lu, ACS Applied Materials & Interfaces 3 (2011) 3078–3083.
[170] S.B. Yang, X.L. Feng, L. Wang, K. Tang, J. Maier, K. Müllen, Angewandte Chemie International Edition 49 (2010) 4795–4799.
[171] S.B. Yang, X.L. Feng, X.C. Wang, K. Müllen, Angewandte Chemie International Edition 50 (2011) 5339–5343.
[172] S.B. Yang, X.L. Feng, K. Müllen, Advanced Materials 23 (2011) 3575–3579.
[173] D.H. Wang, R. Kou, D. Choi, Z.G. Yang, Z.M. Nie, J. Li, L.V. Saraf, D.H. Hu, J.G. Zhang, G.L. Graff, J. Liu, M.A. Pope, I.A. Aksay, ACS Nano 4 (2010) 1587–1595.
[174] Y. Qiu, K. Yan, S. Yang, L. Jin, H. Deng, W. Li, ACS Nano 4 (2010) 6515–6526.
[175] Y. Zou, Y. Wang, Nanoscale 3 (2011) 2615–2620.

Author's personal copy

[176] A. Yu, H.W. Park, A. Davies, D.C. Higgins, Z. Chen, X. Xiao, The Journal of Physical Chemistry Letters 2 (2011) 1855–1860.
[177] C.X. Guo, M. Wang, T. Chen, X.W. Lou, C.M. Li, Advanced Energy Materials 1 (2011) 736–741.
[178] N. Zhu, W. Liu, M.Q. Xue, Z.A. Xie, D. Zhao, M.N. Zhang, J.T. Chen, T.B. Cao, Electrochimica Acta 55 (2010) 5813–5818.
[179] Y. Shi, L. Wen, F. Li, H.M. Cheng, Journal of Power Sources 196 (2011) 8610–8617.
[180] N. Li, G. Liu, C. Zhen, F. Li, L.L. Zhang, H.M. Cheng, Advanced Functional Materials 21 (2011) 1717–1722.
[181] H. Liu, P. Gao, J. Fang, G. Yang, Chemical Communications 47 (2011) 9110–9112.
[182] G. Wang, T. Liu, Y. Luo, Y. Zhao, Z. Ren, J. Bai, H. Wang, Journal of Alloys and Compounds 509 (2011) L216–L220.
[183] J. Yan, Z.J. Fan, T. Wei, W.Z. Qian, M.L. Zhang, F. Wei, Carbon 48 (2010) 3825–3833.
[184] P.V. Kamat, The Journal of Physical Chemistry Letters 1 (2010) 520–527.
[185] Y.Y. Liang, H.L. Wang, H.S. Casalongue, Z. Chen, H.J. Dai, Nano Research 3 (2010) 701–705.
[186] H.L. Wang, J.T. Robinson, G. Diankov, H.J. Dai, Journal of the American Chemical Society 132 (2010) 3270–3271.
[187] M.S. Whittingham, Chemical Reviews 104 (2004) 4271–4301.
[188] D.W. Wang, F. Li, J.P. Zhao, W.C. Ren, Z.G. Chen, J. Tan, Z.S. Wu, I. Gentle, G.Q. Lu, H.M. Cheng, ACS Nano 3 (2009) 1745–1752.
[189] J.J. Xu, K. Wang, S.Z. Zu, B.H. Han, Z.X. Wei, ACS Nano 4 (2010) 5019–5026.
[190] Y.S. He, D.W. Bai, X.W. Yang, J. Chen, X.Z. Liao, Z.F. Ma, Electrochemistry Communications 12 (2010) 570–573.
[191] H.L. Wang, H.S. Casalongue, Y.Y. Liang, H.J. Dai, Journal of the American Chemical Society 132 (2010) 7472–7477.
[192] Z.J. Fan, J. Yan, L.J. Zhi, Q. Zhang, T. Wei, J. Feng, M.L. Zhang, W.Z. Qian, F. Wei, Advanced Materials 22 (2010) 3723–3728.
[193] H.K. Jeong, M. Jin, E.J. Ra, K.Y. Sheem, G.H. Han, S. Arepalli, Y.H. Lee, ACS Nano 4 (2010) 1162–1166.
[194] J. Yan, T. Wei, B. Shao, F.Q. Ma, Z.J. Fan, M.L. Zhang, C. Zheng, Y.C. Shang, W.Z. Qian, F. Wei, Carbon 48 (2010) 1731–1737.
[195] J.K. Lee, K.B. Smith, C.M. Hayner, H.H. Kung, Chemical Communications 46 (2010) 2025–2027.
[196] B. Kang, G. Ceder, Nature 458 (2009) 190–193.

Zhong-Shuai Wu received his Bachelor's degree in Chemistry and Master degree in Inorganic Chemistry from Liaoning University in 2004 and 2007, and Ph.D. in Materials Science from Institute of Metal Research, Chinese Academy of Sciences in 2011 supervised by Prof. Hui-Ming Cheng. He is currently a postdoctoral fellow working with Prof. Dr. Klaus Müllen at Max-Plank Institute for Polymer Research. His research mainly focuses on synthesis and application explorations of graphene and nanomaterials for energy storage and conversion systems in batteries, supercapacitors and fuel cells.

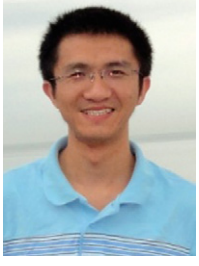

Guangmin Zhou received his Bachelor's degree from the Department of Materials Science and Engineering at Nanjing University of Science and Technology in 2008. He is currently pursuing his Ph.D. under the supervision of Prof. Hui-Ming Cheng at Shenyang National Laboratory for Materials Science, Institute of Metal Research, Chinese Academy of Sciences. His research interests mainly focus on synthesis and application explorations of carbon-based materials for lithium-sulfur batteries and lithium ion batteries.

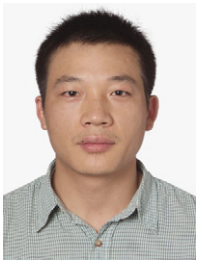

Li-Chang Yin received his Ph.D. in Particle and Nuclear Physics from Jilin University, Changchun, the People's Republic of China, in 2002. He started his postdoctoral work at the Advanced Carbons Research Division, Shenyang National Laboratory for Materials Science, Institute of Metal Research, Chinese Academy of Science from 2003, and then joined its faculty from 2006. He worked at the Tohoku University of Japan in 2009. His research interests center on the theory and computational simulation of low dimensional nano-materials.

Wencai Ren received his Ph.D. degree in materials science from Institute of Metal Research (IMR), Chinese Academy of Sciences (CAS) in 2005. He has been an assistant and associate professor of materials science at IMR, CAS since 2005, and was promoted to be a professor in 2011. From 2009 to 2010, he worked with Prof. Andre K. Geim at the University of Manchester as a visiting researcher. His current research interests include the synthesis, properties and applications of graphene and carbon nanotubes.

Feng Li is a professor of the Institute of Metal Research, Chinese Academy of Sciences (IMR, CAS). He received his Ph.D. in materials science at IMR, CAS in 2001 supervised by Prof. Hui-Ming Cheng. He mainly works on the nanomaterials for clean energy such as electrode materials for lithium ion battery and supercapacitor.

Hui-Ming Cheng received his Ph.D. in Materials Science from the Institute of Metal Research, Chinese Academy of Sciences (IMR, CAS). He worked at AIST and Nagasaki University in Japan, and MIT in USA. Currently he is Professor and Director of the Advanced Carbons Research Division at Shenyang National Laboratory for Materials Science, IMR, CAS. His research interests focus mainly on carbon nanotubes, graphene, high-performance bulk carbons, materials for batteries and electrochemical capacitors, and photocatalytic materials for hydrogen production and CO_2 conversion.